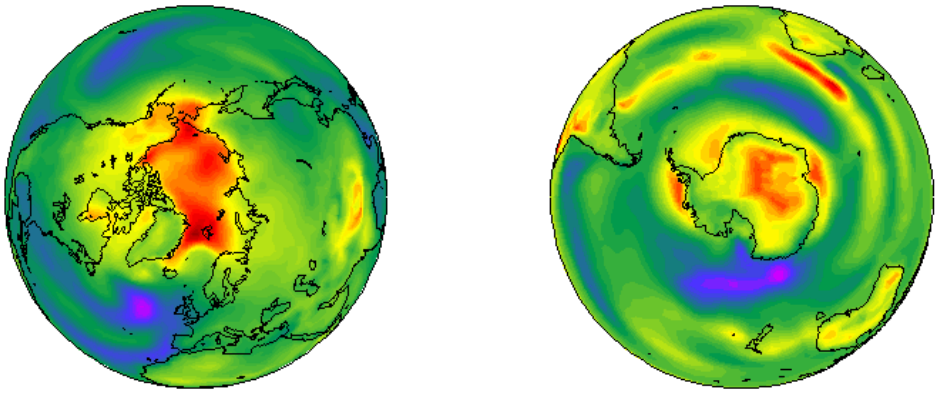

Master OACOS

Final year Research Internship

A new approach of the feedback analysis and its application to the asymmetry of the polar amplification

Author:
Quentin Libois[1]

Supervisors:
Jean-Louis Dufresne[2]
Alain Lahellec[2]

October 20, 2011

[1] Ecole des Ponts ParisTech

[2] Laboratoire de Météorologie Dynamique

CONTENTS

Abstract

Polar observations enhance that global warming in polar regions is much more important than anywhere else on Earth. Models predict Arctic to have a warming twice as large as the average warming whereas in Antarctic models assume a warming of average amplitude. Hence this amplification is asymmetric. We present a feedback analysis method that allows us to compare quantitatively Arctic and Antarctic feedback mechanisms. The albedo feedback is greater in Arctic, where the ocean lays underneath the ice field. Antarctica is more isolated, partly because of the strong heat capacity of the Southern ocean. As it is also a very dry continent, the greenhouse effect there is highly impacted by a small increase in atmosphere water content. Unlike the average on Earth the cloud cover tends to increase in polar regions, so that the clouds albedo effect can counterbalance the increased greenhouse effect due to high altitude clouds. In this report, we focus on the apparent linearity of the climate in General Circulation Models (GCMs). We make an analogy between a simple electrical circuit and the climate response to an external forcing. Such an analogy allows us to characterise the complex climate system with only a few parameters that can be deduced from the thorough study of the model outputs (namely the feedback parameter and the ocean heat efficiency). Using this analogy we test the effective linearity of the Institut Pierre Simon Laplace (IPSL) model. We also highlight the existence of two characteristic times in the climate, of approximatively 15 and 400 years. Following this linearity argument, we develop a diagnostic way of evaluating climate feedbacks from a perturbed climate run. We quantify the feedback parameters of the IPSL model, and obtain similar results as former studies, except that in our simulations, clouds seem to have a greater impact, and water vapour a lower one than usually. The same method was applied to polar regions.

INTRODUCTION

This work focuses on climate feedbacks and the way to define, identify and quantify them. We use the IPSL GCM but our methods might be applied to any GCM. We work with two main simulations: the ramp experiment and the step experiment. The first corresponds to a linear increase of the CO_2 forcing with time (ie a $1\%.\text{yr}^{-1}$ increase in CO_2 concentration), up to a quadrupling after 140 years. The step experiment consists in an instantaneous quadrupling of CO_2 in the atmosphere from a pre-industrial reference concentration. We analyse the evolution of the climate system during 250 years onward. First, we describe the vocabulary of feedback analysis in chapter 1. We highlight that since the first feedback analysis (see Hansen et al. [1984]) an hypothesis of linearity is made on the climate response to an external forcing. This has been used in several articles since (see Gregory and Mitchell [1997], Gregory et al. [2004] or Dufresne and Bony [2008]). We present in chapter 2 a very simple linear electrical circuit that illustrates the behaviour of such a GCM forced by a step or a ramp forcing. It provides a more general interpretation of the classical assumed linearity. The electrical circuit represents an energy budget of the Earth, composed of an atmosphere, an ocean mixed layer and a deep ocean. From this analogy, we deduce physical equations and characteristic times. We get that for sufficiently small changes in surface temperature, the evolution of any physical quantity with time for a step forcing follows an exponential law. In fact, we define two typical time-scales of the climate system, a short one related to the surface ocean and the continents and a longer one representing the inertia of the whole deep ocean. We also point out that a very short time-scale must exist and is representative of the atmospheric time-scales, shorter than one year. From the decomposition of the time evolution of ΔT on these two various time-scales, we highlight the fundamental meaning of a transient temperature and show how committed temperature change can be evaluated.

In chapter 3, following Gregory and Webb [2008], we decompose the climate response to an external forcing (here an increase in atmospheric CO_2) in terms of

rapid forcings and slow feedbacks. We show that part of the response is a direct consequence of the anthropic forcing and occurs very quickly, while the rest of the response is proportional to the surface temperature change. Differentiating these two components is essential since it defines the effective sensitivity of a feedback mechanism. We highlight fundamental issues that have been already discussed in Soden and Held [2006] and Soden et al. [2008].

The previous analysis leads us to define a new way of evaluating the climate feedbacks in GCMs. Contrary to Partial Radiative Perturbation (PRP) methods that do not necessarily differentiate the slow and fast responses of the climate and are based on irrealistic climate evolutions, we propose a method based on an accurate study of the flux during the ramp experiment. Reasoning in terms of flux allows us to attribute a change in the top of atmosphere (TOA) energy budget to a given mechanism. Thus we have the effective contribution of each feedbacks resulting from a climate simulation. We compare the results to former studies presented in Soden and Held [2006] and Soden et al. [2008]. Our method has the advantage of being computationally light but we highlight that the longwave decomposition of the net TOA flux is difficult.

Eventually, we apply the results of this work to the analysis of the polar amplification. It has often been studied in terms of particular feedbacks (the albedo issue has been tackled in Hall [2004], Winton [2006] and Boé et al. [2009], heat transport in Cai [2005] and Langen and Alexeev [2007]). We analyse it both in terms of quantitative warming and in terms of its origins. We focus on the differences between Arctic and Antarctica, more specifically on their typical time scales and on the physical mechanisms implied. We highlight the fundamental roles of albedo and water vapour in the asymmetry of the amplification.

CHAPTER 1

GENERAL NOTIONS ON CLIMATE FEEDBACKS

In this chapter, we introduce the notions of feedback parameters and forcings for a climate simulation. These concepts are essential to understand the response of a climate system to an external radiative perturbation.

1.1 The feedback parameter λ

In response to an external forcing such as a solar irradiance increase or an input of anthropic greenhouse gases into the atmosphere, the Earth tends to warm up. In fact, to be at equilibrium, thermal radiation from the Earth at TOA must balance the external radiation increase. At any time we can define the net radiative flux (in $\mathrm{W.m^{-2}}$, positive downward) at TOA N as the algebraic sum of the forcing ΔQ, and the Earth radiative response that is assumed proportional to the change in surface temperature ΔT_s, later called ΔT. We write the first-order energy balance:

$$N = \Delta Q - \lambda \Delta T_s \tag{1.1}$$

λ is called the feedback parameter (in $\mathrm{W.m^{-2}.K^{-1}}$) and is the reciprocal of the climate sensitivity. Indeed, the larger λ, the smaller ΔT must be to balance the forcing. Equation 1.1 expresses an energy conservation and thus must be applied to an horizontally isolated region. This is true for fluxes averaged on Earth but further we will treat the case of local isolated areas.

At general equilibrium, when $N = 0$, 1.1 becomes:

$$\Delta Q = \lambda \Delta T_{s,eq} \tag{1.2}$$

where $\Delta T_{s,eq}$ is the average change in surface temperature at equilibrium (from now on we call it simply ΔT_{eq}). λ will be considered constant in time for a given model unless the contrary is mentioned.

It is well-known that GCMs yield warming greater than the simple black-body warming that would result if the climate system did not respond to radiative external forcings. This amplified temperature response is due to feedback mechanisms that in average amplify the Earth response through complex climate dynamics. The Planck feedback parameter λ_p is the value that λ would have for an inert climate. We call ΔT_0 the resulting change in surface temperature that would result for such a system:

$$\Delta Q = \lambda_p \Delta T_0 \tag{1.3}$$

Let's call T_e the earth's equivalent black body temperature, corresponding to the temperature emission seen from space. For a vertically homogeneous increase in temperature ΔT_0 and using Stefan's law, we have:

$$F = \sigma T_e^4 \Longrightarrow \Delta F = 4\sigma T_e^3 \Delta T_e = \lambda_p \Delta T_0 \tag{1.4}$$

where F is the radiative emission of the Earth towards space. From 1.4 we infer the value of λ_p that will be taken from now on as $\lambda_p = 3.2\text{W.m}^{-2}\text{.K}^{-1}$ [1]. The tiny difference between ΔT_e and ΔT_0 comes from the non-linearity of Stefan's law [2].

To evaluate the impact of the climate in terms of radiative response, we introduce the net feedback factor f such as:

$$\Delta T_{eq} = f \Delta T_0 \tag{1.5}$$

$f \geq 1$ means that climate processes amplify the warming experienced by the Earth compared to a climatologically inert planet.

From Eqs. 1.5 and 1.2 be can write:

$$f = \frac{\lambda_p}{\lambda} \tag{1.6}$$

Various physical processes participate to the climate response. The feedback parameter λ can be split up into several components, namely Planck black body (P), lapse rate (LR), clouds (C), water vapour (WV) and surface albedo (SA) effects. These mechanisms can affect either shortwave (SW), or longwave (LW) domains. We can now write:

$$\lambda = \lambda_P + \lambda_{LR} + \lambda_C + \lambda_{WV} + \lambda_{SA} \tag{1.7}$$

[1] This is the average value found in Soden and Held [2006] for instance. There is few disparity within the models for this value obtained by radiative transfer calculations, that is why we consider it as a constant

[2] Indeed, for a vertically homogeneous increase of the atmosphere temperature lower layers emission increases more than that of the upper ones. This results in a natural greenhouse effect and hence the radiative equivalent temperature does not increase as much as the surface one. More details are given in Appendix C

It becomes interesting to decompose f the same way:

$$f = 1 + f_{LR} + f_C + f_{WV} + f_{SA} \tag{1.8}$$

We also introduce the gains g_i for each feedback mechanisms. They compare the intensity of a feedback to Planck feedback:

$$g_i = -\frac{\lambda_i}{\lambda_P}$$
$$g_{tot} = \sum_{i \neq P} g_i$$

Dividing Eq. 1.7 by λ_P we get:

$$f = \frac{1}{1 - g_{tot}} \tag{1.9}$$

$$f = 1 + \frac{\sum_{i \neq P} g_i}{1 - g_{tot}} \tag{1.10}$$

Identifying with Eq. 1.8 and we get the expression of f_i in function of the g_i:

$$f_i = \frac{g_i}{1 - g_{tot}} \tag{1.11}$$

1.2 Nature of the feedbacks

In this section we define physically and very simply the various feedback mechanisms introduced in the previous section. We highlight the fact they are effectively strongly bound to the surface temperature.

Temperature feedbacks

Given Stefen's law, an increase of surface temperature tends to counterbalance the imposed forcing at TOA since it increases the Earth radiative emission. This is referred to as the Planck feedback.

The lapse rate is the vertical gradient of temperature from the ground to TOA. The greater (the more negative) this gradient is, the lesser LW radiations are emitted since the Earth equivalent temperature is diminished. Changes in surface temperature can modify this lapse rate through various mechanisms such as convection or absorption. The two effects of temperature are rather difficult to differentiate in climate simulations. The Planck effect will refer to the impact of a vertically uniform change in temperature whereas the lapse-rate effect highlights changes in the lapse-rate itself. This difference is illustrated on figure 1.1.

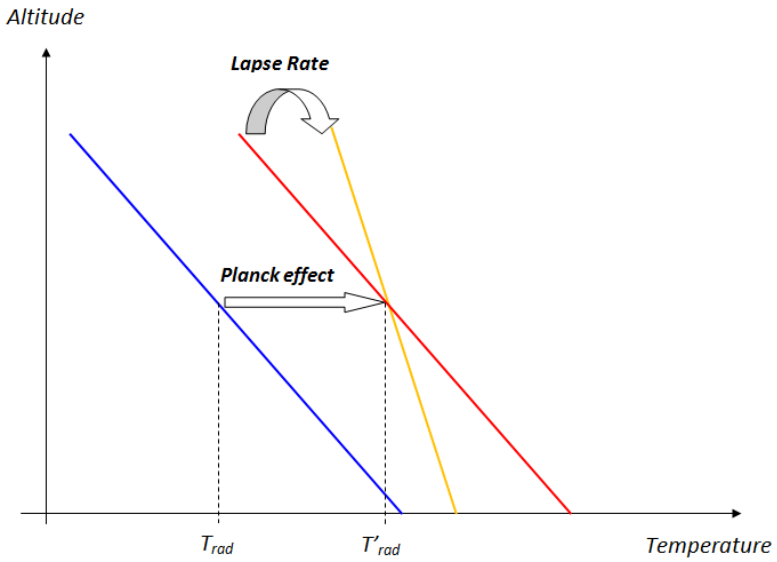

Figure 1.1: Scheme illustrating Planck and Lapse Rate effects (T_{rad} is the radiative equivalent temperature seen from space)

Water vapour

Water vapour is the most important greenhouse gas in the atmosphere. At a higher temperature the atmosphere can hold more water vapour. This comes from Clapeyron's law (see figure 1.12, where p_{eq} gives the saturation pressure of a gas as a function of temperature, p_{ref} and T_{ref} are reference values, L and R are the latent heat of vaporization and the gas constant). Surface warming enhances the greenhouse effect of water vapour, which reduces the global emission of LW radiation from the Earth.

Clouds

Changes in cloud cover and altitude can both change the reflection of SW solar radiation, thus modifying the surface downward SW radiation (this is the clouds albedo effect), but they also cause greenhouse effect by absorbing LW radiation. This points out the role of clouds in both SW and LW budget and the consequent complexity of clouds as a climatic object. In fact the feedback of clouds is very uncertain and λ_C covers a wide range of values among current GCMs (see Soden and Held [2006]).

Surface Albedo

Eventually, changes in surface albedo (the surface efficiency to reflect SW radiation) also modifies the Earth radiative budget. It is clear that the Earth albedo depends

$$p_{eq}(T) = p_{ref} \exp\left(\frac{L}{R}\left(\frac{1}{T_{ref}} - \frac{1}{T}\right)\right) \tag{1.12}$$

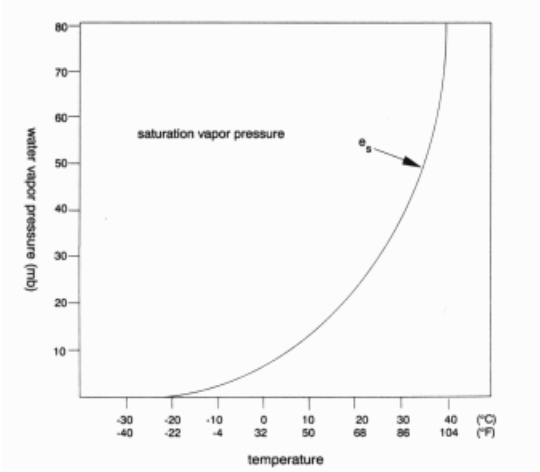

Figure 1.2: Clapeyron's law and its graphic representation

on surface temperature, particularly as far as snow and ice albedos are concerned.

A more detailed analysis of the nature of these feedbacks is given in Bony et al. [2006] which describes precisely all these phenomena and the corresponding uncertainties on their role in climate warming.

1.3 Positive and negative feedbacks

It is clear that some phenomena will amplify the initial perturbation in temperature (they are called positive feedbacks) whereas others will dampen this increase (they are negative feedbacks). If R is the radiation lost by the Earth ($R = \lambda \Delta T$), then a mechanism will have a positive feedback (namely $\lambda \leq 0$) if its contribution to R decreases for an increase in T. To evaluate the sign of a feedback, it is relevant to decompose the derivative of R over T into the sum:

$$\frac{dR}{dT} = \sum_i \frac{dR_i}{dT} \tag{1.13}$$

$$= \sum_i \frac{\partial R}{\partial x_i} \frac{dx_i}{dT} \tag{1.14}$$

where the x_i represent the various processes. Note that in this decomposition, the processes are independent from each other and depend only on the temperature. For instance, if x_{wv} is the quantity of water vapour in the atmosphere, we have given previous section:

$$\left.\begin{array}{ll} \dfrac{\partial R}{\partial x_{WV}} & \leq 0 \\ \dfrac{dx_{WV}}{dT} & \geq 0 \end{array}\right\} \Longrightarrow \lambda_{WV} = \frac{dR_{WV}}{dT} \leq 0$$

and thus water vapour has a positive feedback on climate change. Applied to the others mechanisms, one might find that Planck and LR effects have negative feedbacks whereas SA has a positive one. The effect of clouds is rather unclear since they interact with both LW and SW radiation and their effects depend on their altitude, nature and temperature.

1.4 Attributing a change in temperature to a mechanism

We have explained that due to climate processes, the global change in temperature is the result of a sum of mechanisms. Current works focus on the evaluation of the feedback parameters. In other terms, it seems interesting to decompose ΔT into a sum of various ΔT_i, each one attributed to a given physical process. This decomposition was formally done in Dufresne and Bony [2008]. The authors proved that each contribution depends on the feedback gain:

$$\Delta T_i = g_i \Delta T \tag{1.15}$$

1.5 The regression method

Although it will reveal difficult to evaluate each of the λ_i we show that a very simple method allows us to evaluate the values of ΔQ and λ in equation 1.1.

In a climate simulation, N can be computed since it is the algebraic sum of outgoing and ingoing SW and LW flux at TOA. N can also be measured with satellites (this was the goal of the Earth Radiative budget Experiment (ERBE)) and it gives important information on the way the Earth redistributes the incoming solar energy. Equation 1.2 shows that knowing N, ΔQ and ΔT at any time of a transient experiment, one can deduce the sensitivity λ which is in practice a precious quantity. For instance, in an abrupt step experiment, ΔQ is fixed by the amount of CO_2 introduced in the atmosphere, but also represents quick modifications in the radiative budget which do not depend on surface temperature variations (this point will be discussed in chapter 3). Plotting N versus ΔT gives the respective values of λ (slope) and ΔQ (y-intercept). This method was first proposed in Gregory and Mitchell [1997] and will be applied to other quantities later on. From now on we call it the regression method. From figure 1.3 we evaluate the global feedback parameter $\lambda = 0.77\text{W.m}^{-2}\text{K}^{-1}$ ($\pm 10\%$) and $\Delta Q = 6.5\text{W.m}^{-2}(\pm 10\%)$ for the IPSL model. We use globally averaged values for the temperature and the net flux and used 4-year mobile averages to smooth the plot. Since we considered λ to be constant with time in this part, the equilibrium temperature ΔT_{eq} can be interpolated from the same

regression by prolonging the line to $N = 0$. We find $\Delta T_{eq} = 8.4\text{K}(\pm 10\%)$. In table 1.5 we provide the characteristics of the IPSL model obtained for the actual and former models. Applying this method to various models would give a comparison of the feedback parameters of these very models, which is an issue at stake for studies such as IPCC reports (Solomon et al. [2007]).

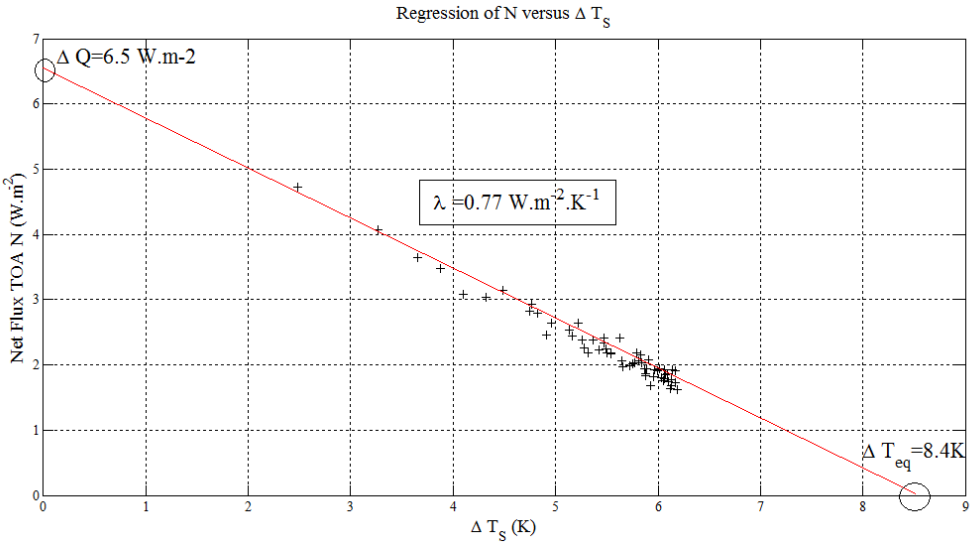

Figure 1.3: The regression used to determine λ, ΔQ and ΔT_{eq}

	λ (W.m^{-2}.K^{-1})	ΔQ (W.m^{-2})	ΔT_{eq} (K)
Actual model	0.77	6.5	8.4
Former model	0.78	6.3	8

Table 1.1: Characteristics of the actual and former IPSL models obtained by the regression method

CHAPTER 2

AN ELECTRICAL ANALOGY OF THE FEEDBACK ANALYSIS

In this chapter we present a simple linear model of the climate by making an analogy between the climate system and an equivalent electrical circuit. We show that such a basic model gives an understanding of some well-known results and we use it to describe quantitatively the parameters of the IPSL model.

2.1 At equilibrium

Starting from the set of equations displayed in chapter 1, we want to make the relations between f, g, ΔT_S and ΔQ more visual.

At equilibrium, equalities 1.2 and 1.3 hold and:

$$\Delta T_{eq} = f \Delta T_0 = f \frac{\Delta Q}{\lambda_p} \tag{2.1}$$

Given $f = 1 + \sum_i f_i$ we can write:

$$\Delta Q = \frac{\lambda_p}{1 + \sum_i f_i} \Delta T_{eq} = \frac{1}{\frac{1}{\lambda_p} + \sum_i \frac{1}{\frac{\lambda_p}{f_i}}} \Delta T_{eq} \tag{2.2}$$

The latter equality can be seen as a Ohm law, where ΔQ is an imposed tension (a forcing) and ΔT_{eq} the resulting intensity in the circuit due to this forcing. We manipulated the equality in order to put forward the expression of a parallel resistive circuit. In fact, if we define the resistivity

$$R_i = \frac{\lambda_p}{f_i}$$

it is clear that the climate feedback analysis is equivalent to the electrical circuit of figure 2.1 (where only the Planck response and two feedbacks are represented). Note that R_i here is different from R_i in 1.14.

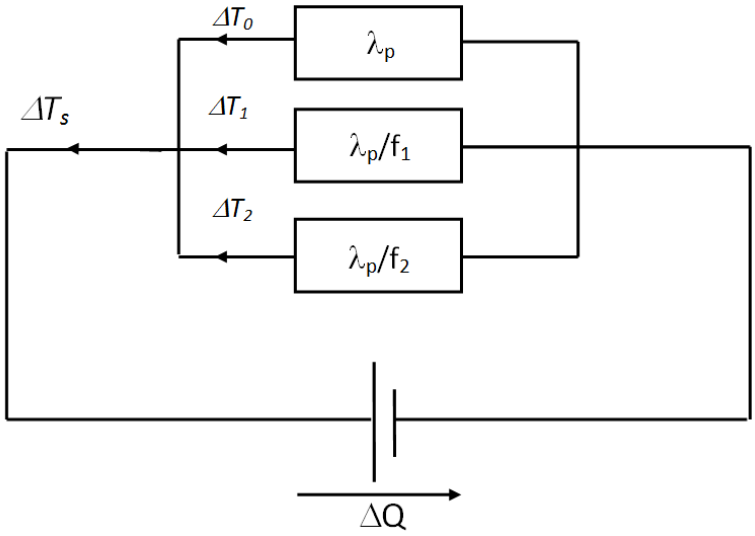

Figure 2.1: Electrical circuit used for the analogy at equilibrium

An interesting point of representing the feedbacks as a parallel resistive circuit is to see their imbrication. First of all, it is very easy to calculate the intensity exiting the resistance R_i:

$$\Delta T_i = f_i \frac{\Delta Q}{\lambda_p} = f_i \Delta T_0 = g_i \Delta T_{eq} \tag{2.3}$$

This representation highlights clearly the contribution of each feedback to the global ΔT_s. We find the previous relation 1.15. Each f_i depends on the other feedbacks through g_{tot} (see Eq. 1.10), meaning that removing a feedback would perturb the whole feedback mechanisms. It is a way to explain that feedbacks cannot be taken separately one from the others, at least in terms of temperature change. If a feedback becomes stronger, the consequent change in temperature will enhance other feedbacks which reactions will amplify the initial perturbation. The complexity of isolating the feedback mechanisms in terms of feedback loops is tackled in Lahellec and Dufresne [2011].

2.2 Transient regime

Another point that has been discussed since the original paper Hansen et al. [1984] is the transient response of the climate system to a radiative perturbation. In the latter paper, the authors suggested that the response time would be determined by the heat capacity of the ocean mixed layer. With an average value of about 60m, the response time of the ocean to an increase in surface temperature would be of some 10 years, that is found for slab ocean simulations. This is evaluated using the approximation that the net flux TOA is transferred to the ocean and warms up the mixed layer. Thus, using the flux balance, we have

$$N = \Delta Q - \lambda \Delta T(t) = \frac{d}{dt}(C_s \Delta T(t)) \tag{2.4}$$

where C_s is a heat capacity per surface unity (in J.K^{-1}.m^{-2}) which yields a characteristic time τ equal to $\frac{C_s}{\lambda}$. As $f = \frac{\lambda_p}{\lambda}$ we notice that

$$\tau_f = f\tau_0 \tag{2.5}$$

with τ_0 the response time in a no-feedback analysis. In fact, due to feedback mechanisms, the climate requires more time to adjust to a forcing.

Once more, from equation 2.4 we can find an equivalent circuit. It is obtained in adding to the initial circuit a coil that represents the mixed layer inertia. We represented it on figure 2.2 From this RL circuit, the characteristic time is particularly easy to find. It is given by $\tau = \frac{L}{R}$ and the results established in Hansen et al. [1984] appear clearly as characteristics of the circuit described.

At this point, it has to be noticed that the effective response time of Earth to an external forcing in Atmosphere Ocean coupled model is rather several centuries than decades. This shows that the equilibrium also requires a modification of the deeper ocean. At shorter term only the surface mixed layer might be perturbed by the forcing ΔQ but on longer times scales, the whole ocean should be considered to reach an hypothetical ultimate equilibrium state.

2.3 The deep ocean

2.3.1 The energy budget of the ocean

To represent the role of the deeper ocean in our simplistic model, we take into account the result provided by Gregory and Mitchell [1997]. For an Atmosphere Ocean coupled GCM (AOGCM) and for a linear increase of ΔQ with time (resulting from an exponential increase in atmospheric CO_2 concentration), it is observed that ΔT and N both evolve linearly with time. We can assimilate N to the net flux into the ocean, as long as the heat capacity of the atmosphere is neglected. Classically a coefficient κ called ocean heat efficiency is introduced as

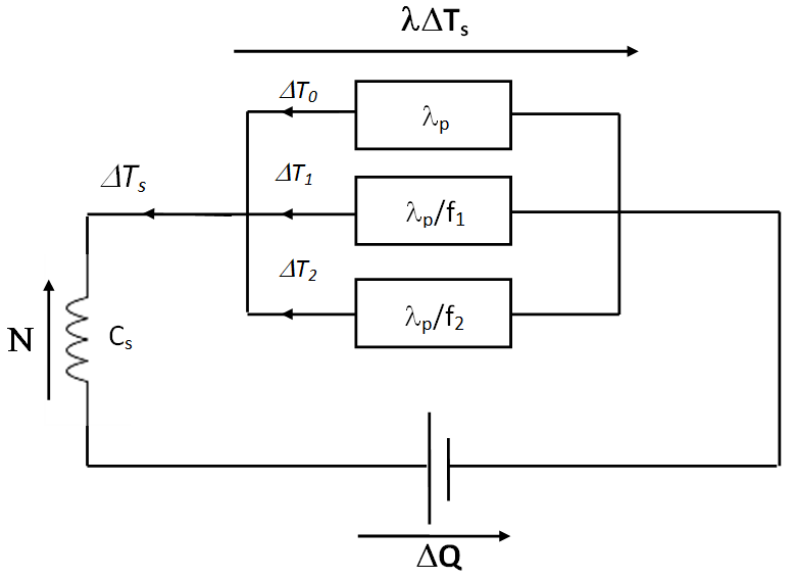

Figure 2.2: Electrical circuit used for the analogy including the ocean mixed layer

$$N = \kappa \Delta T \tag{2.6}$$

This relation is almost observed in the current IPSL model for the ramp experiment and is represented on figure 2.6. Nonetheless, the linear relation is not exact at the beginning of the experiment. Extrapolating linearly the curve from longer times, we get a non-null y-intercept. This was not seen in Gregory and Mitchell [1997] but cannot be ignored in the experiments used for this work.

In fact, relation 2.6 suggests that the system moves away from its equilibrium state. However, for small perturbations, one might suppose the system would reach a dynamic equilibrium state, for instance a state in which N remains constant, meaning that the system responds to the increasing forcing with some time-lag. From this physical question, we pretend that the apparent linearity of N with time is only the first order approximation (at short term) of an exponential term that would tend toward a constant. This has sense since the simulations which led to the expression 2.6 were run on a century more or less which is much smaller than the approximative global time scale of several centuries given by Schwartz [2007], Wetherald et al. [2001] or Stouffer [2004]. Moreover, the net flux into the ocean logically increases before the surface temperature can react so the profile presented on figure 2.6 seems more relevant. It is clear that Eq. 2.6 is untrue for both very short and very long times. To implement this new observation in our circuit, we are looking for a representation that does not modify the equilibrium state but controls the transient regime.

We propose a simple model in which the net flux TOA heats the ocean, the latter composed of a surface layer and a deep ocean that can store the energy transferred

from the surface through a flux-gradient process:

$$F = \kappa(\Delta T - \Delta T_d) \tag{2.7}$$

where ΔT_d is the temperature of the deep ocean. Relation 2.6 holds only if the heating of the surface layer is negligible and the deep ocean has not yet warmed up. The scheme and the circuit we propose are represented on figure 2.3. C_d represents the heat capacity of the deep ocean, while C_s corresponds those of the surface mixed layer. Numerically, $C_d \gg C_s$. We also introduced different temperatures for the surface (T_s) and the deep ocean (T_d). We give in appendix A a physical interpretation of the empirical coefficient κ.

Straight away we observe that at equilibrium the circuit comes down to the one shown on figure 2.1 since the coils become wires. With such a circuit, for short times (compared to the response time of the deep ocean discussed further) we find the relation 2.6 and for longer time the deeper ocean accounts for an immense heat capacity. Let say that in the model, we do not consider the feedbacks to have proper self-inductances, since atmospheric feedbacks react much more rapidly than the ocean (months or years vs decades). A complete analysis would require, for shorter time analysis, the serial addition of self-inductances besides the feedbacks resistances. In a word, we only treat with this model the part of the climate response that occurs for times longer than the atmospheric or continental inertia time. Let say that the inductance of the atmosphere is so small that it very quickly behaves like a wire.

2.3.2 Differential equation of the circuit

Now that we have a complete electrical circuit, we will establish its equations in order to define typical time scales. We will then compare the theoretical responses of the circuit to the results of the GCMs simulations, both for a step and a ramp forcing. For convenience, we use electrical terms which highlight the correspondence between climate physical properties and their electrical equivalent. Thus the final electrical circuit is given by figure 2.4.

Remark: The choice of inductances in our circuit is due to its visual interest. In fact, it is clear that a more classical circuit with condensers instead of shelves would be correct (it is represented on figure 2.4). Nonetheless, the addition of the intensities in our scheme puts clearly forward the additivity of the various feedbacks (in the equivalent circuit with condensers the tensions would add linearly).

Now we obtain the set of equations for this circuit (notations are coherent with figure 2.3 (left):

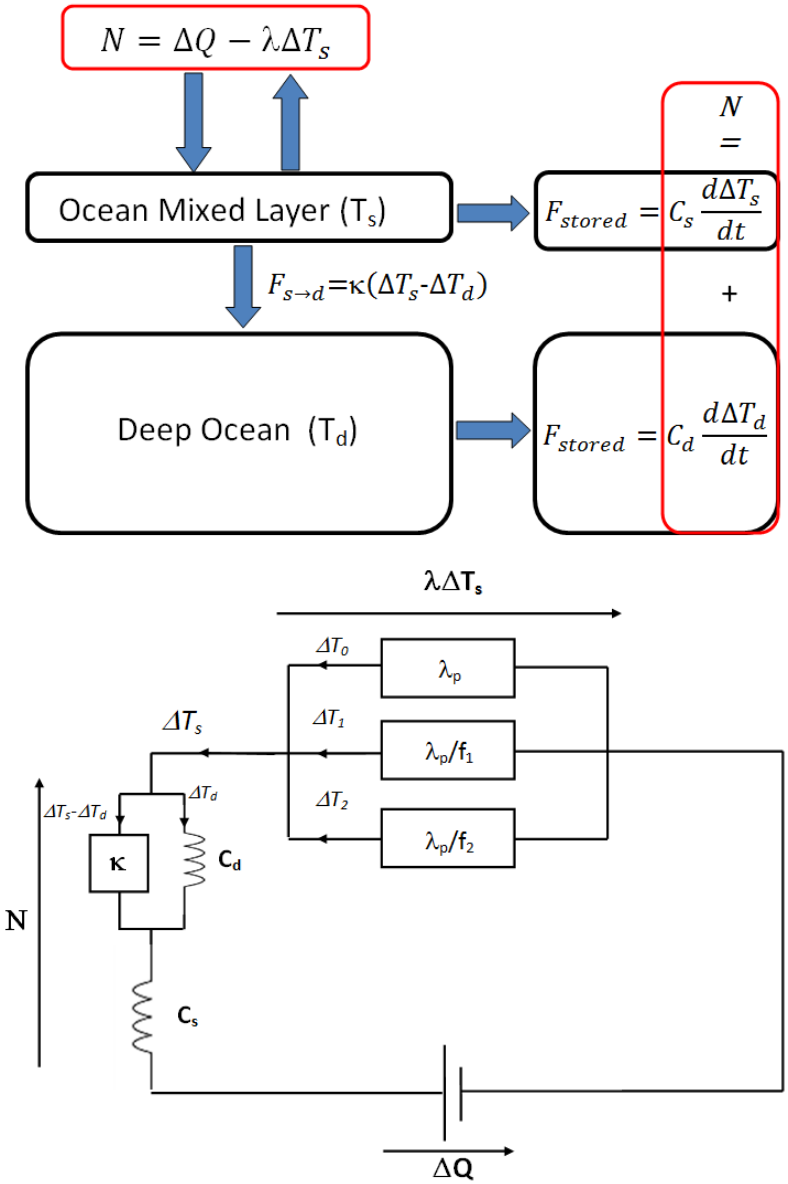

Figure 2.3: The energy scheme and the final electrical circuit used for the analogy

$$U_0 = U_1 + U_2$$
$$i = i_1 + i_2$$
$$U_1 = R_d i_1$$
$$U_1 = L_d \frac{di_2}{dt}$$

$$U_2 = \left(R + L_s \frac{d}{dt}\right) i$$
$$L_d \frac{di}{dt} = \left(R_d + L_d \frac{d}{dt}\right) i_1$$
$$U_0 = \left(R + L_s \frac{d}{dt}\right) i + R_d i_1$$

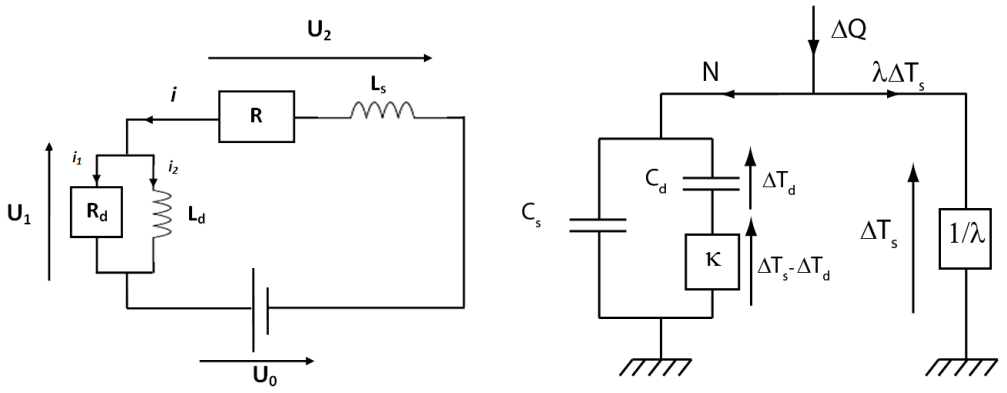

Figure 2.4: Final electrical circuit used for the analogy. With coils (l.) or capacities (r.)

Applying the operation $\left(R_d + L_d \frac{d}{dt}\right)$ on the last equality, we obtain:

$$\left(R_d + L_d \frac{d}{dt}\right) U_0 = \left(R_d + L_d \frac{d}{dt}\right) \left(R + L_s \frac{d}{dt}\right) i + R_d L_d \frac{di}{dt} \tag{2.8}$$

We can sort the terms in this equation and now focus on the right-hand term A (after dividing by $L_s L_d$) to define time scales:

$$A = \frac{d^2 i}{dt^2} + \left(\frac{R + R_d}{L_s} + \frac{R_d}{L_d}\right) \frac{di}{dt} + \frac{R R_d}{L_d L_s} i \tag{2.9}$$

We calculate the discriminator of this equation, using $R_{eq} = R + R_d$:

$$\Delta = \left(\frac{R_{eq}}{L_s}\right)^2 \left(1 + \frac{L_s R_d}{R_{eq} L_d}\right)^2 - 4 \frac{R R_d}{L_d L_s} \tag{2.10}$$

Comparing the heat capacity of the mixed layer and the global ocean, we deduce that $\frac{L_s}{R_{eq}} \ll \frac{L_d}{R_d}$ which allows us to develop the expression in Taylor series:

$$\Delta \simeq \left(\frac{R_{eq}}{L_s}\right)^2 \left(1 + 2 \frac{L_s R_d}{R_{eq} L_d} - 4 \frac{R R_d L_s}{L_d R_{eq}^2}\right) \tag{2.11}$$

Eventually we obtain the the values of $x_{1,2} = \tau_{1,2}^{-1}$ (where $\tau_{1,2}$ are the time scales of the system):

$$x_{1,2} = \frac{1}{2} \left(-\frac{R_{eq}}{L_s} \left(1 + \frac{L_s R_d}{R_{eq} L_d}\right) \pm \frac{R_{eq}}{L_s} \sqrt{\left(1 + 2 \frac{L_s R_d}{R_{eq} L_d} - 4 \frac{R R_d L_s}{L_d R_{eq}^2}\right)}\right) \tag{2.12}$$

Thus

$$tau_1 = -\frac{L_s}{R_{eq}} \tag{2.13a}$$

$$tau_2 = -\frac{L_d R_{eq}}{R R_d} \tag{2.13b}$$

Finally, we give the expression of $\Delta T(t)$:

$$\Delta T(t) = A\left(1 - \exp\left(-\frac{t}{\tau_1}\right)\right) + B\left(1 - \exp\left(-\frac{t}{\tau_2}\right)\right) \tag{2.14}$$

where τ_1 and τ_2 are respectively the short and long characteristic times and $A+B = \Delta T_{eq}$ the equilibrium temperature change.

We can also get the expression of N from equality 1.1:

$$N(t) = \lambda\left(A\exp\left(-\frac{t}{\tau_1}\right) + B\exp\left(-\frac{t}{\tau_2}\right)\right) \tag{2.15}$$

From the previous expressions of ΔT and N we deduce that theoretically, the pre-exponential coefficients of N equal λ times those of ΔT, so that we can introduce (it will be essential in forthcoming sections):

$$A_N = \lambda A_{\Delta T} \tag{2.16}$$

$$B_N = \lambda B_{\Delta T} \tag{2.17}$$

Numerical analysis

We can now evaluate the respective values of λ, κ, C_s and C_d. We consider the mixed layer to be 60m deep in average, which is equivalent to an aquasphere with a mixed layer of 40m. We consider an average depth of the ocean of 2700m. Thus $C_s = 1.8 \times 10^8 \mathrm{W.m^{-2}.K^{-1}}$ and $C_d = 1.13 \times 10^{10} \mathrm{J.m^{-2}.K^{-1}}$. We got from the IPSL simulations $\lambda = 0.77 \mathrm{W.m^{-2}.K^{-1}}$ and $\kappa = 0.43 \mathrm{W.m^{-2}.K^{-1}}$.

We evaluate the two characteristic times:

$$\tau_1 = 4.8\mathrm{yrs} \tag{2.18}$$

$$\tau_2 = 1300\mathrm{yrs} \tag{2.19}$$

Let's notice that if this model were used to compare characteristic times of various GCMs, C_s and C_d would be the same for all models, whereas λ and κ would depend on the very model studied. Here is a way to bound the characteristic time scales provided by models to quantities that can be obtained by various regressions. The long characteristic time fits well to the values proposed by the works cited previously. Given that the inertia of the atmosphere is not taken into account, the shorter response-time can be considered as an inferior limit of its real value. Indeed, some characteristic time of $10 - 15$ years would be no surprise and correspond more to what will be observed later on.

An energetic point of view

The electrical circuit can also be interpreted in terms of energy conservation. From figure 2.4 we see that the energy brought by the sun is either sent back by the Earth through feedbacks, or stored in the ocean (in our model, we neglected the heat capacity of the atmosphere). This energy can be stored either in the mixed layer or in the deeper ocean. This amount of energy can be easily calculated from the formula:

$$E = \frac{1}{2} L i_f^2 \tag{2.20}$$

$$E = \frac{1}{2} C U_f^2 \tag{2.21}$$

2.4 Manipulating the electrical model

2.4.1 The apparent linearity of the GCM

We have used a linear electric model to represent a GCM behaviour. This sounds perturbing since a complex climate model is essentially non-linear due to clouds, ice sheets or water thermodynamics. Nonetheless, experiments provide outputs that definitely seem linear and the usual energy balance equations assume that the climate response to small perturbations is linear with these very perturbations. This is true only for large scales and is evidently false at reduced scales. An important application of this apparent linearity is that the step forcing solution might easily give the ramp experiment solution. Indeed, a ramp is nothing but the integral of a step with time. Formally, let say that the solution ΔT of expression 2.14 verifies:

$$\mathcal{F}(\Delta T_{step}) = \Delta Q_{step} \tag{2.22}$$

where $\mathcal{F}$ is a linear operator representing the differential equation.

Integrating the latter identity along time t and dividing by t_f the length of the ramp experiment we get

$$\frac{1}{t_f} \int_0^t \mathcal{F}(\Delta T_{step}) = \int_0^t \frac{\Delta Q_{step}}{t_f} = \Delta Q_{step} \frac{t}{t_f} = \Delta Q_{ramp} \tag{2.23}$$

As the integration operation is linear we can say that $\Delta T_{ramp} = \frac{1}{t_f} \int_0^t \Delta T_{step}$ is the solution in temperature for a ramp forcing that verifies $\mathcal{F}(\Delta T_{ramp}) = \Delta Q_{ramp}$. To support this we plotted on figure 2.5 both terms of the previous equation. We see that there is an excellent correlation between them. Thus, from expression 2.14 we can evaluate the ramp solution easily. For $\tau_1 \ll t \ll \tau_2$ we show in Annex B that:

$$\Delta T_{ramp} = \frac{1}{t_f}\left[A\left(t-\tau_1\right)\right] \tag{2.24}$$

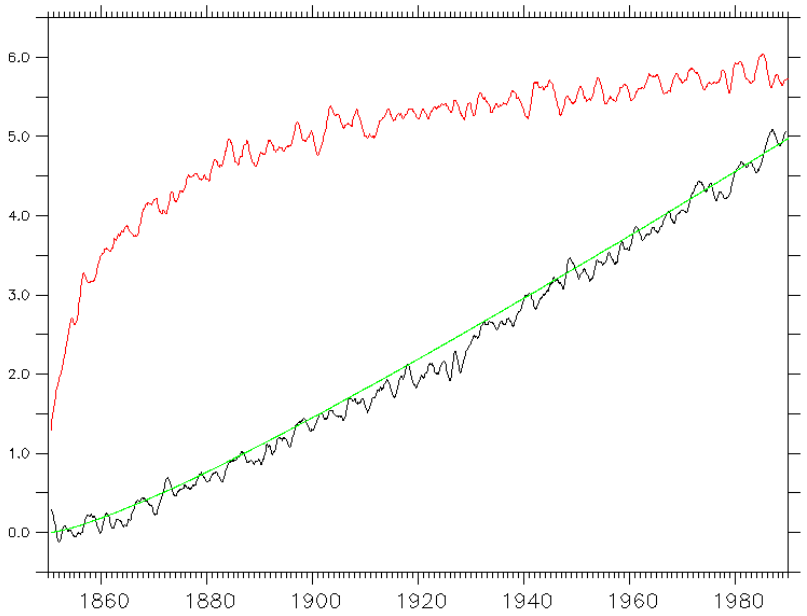

Figure 2.5: Evolution of ΔT for the ramp (black) and step (red) experiments. In green we plotted $\frac{1}{t_f}\int_0^t \Delta T_{step}$

We present on figure 2.7 (left) the experimental evolution of ΔT for the ramp experiment that fits quite well with the expression given above. This expression is also consistent with the fact that at time τ_1 the temperature is almost unchanged since only the atmosphere has responded to the forcing but not the whole ocean mixed layer. It is also important to see that at the end of the ramp experiment, the change in temperature is more or less A which corresponds to the short time scale response of the climate. We conclude that the ramp experiment selects the short time scales since the deep ocean never has time to adjust to the constantly evolving forcing. We can also calculate N in order to compare it to ΔT (also in Annex B). We find the following theoretical relation:

$$N = \kappa\Delta T + \frac{\tau_1}{t_f}\lambda\Delta T_{eq} \tag{2.25}$$

which corresponds to the experimental relation plotted on figure 2.6. It highlights that the relation $N = \kappa\Delta T$ that is often used is not correct. Note that in Dufresne

and Bony [2008] or Gregory and Mitchell [1997] it was calculated at the end of the ramp experiment as $\frac{N_f}{\Delta T_f}$ which would have given $\kappa = 0.56$ in our case. The fact that our physically based analogy reproduces the features of GCMs simulations supports the physical interpretation of κ.

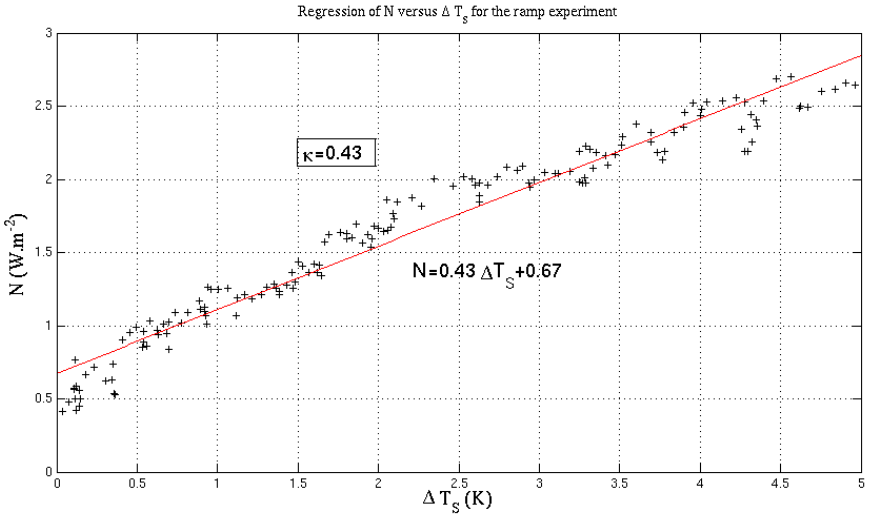

Figure 2.6: Plot of N versus ΔT for the ramp experiment: the ocean heat uptake efficiency κ is given by the slope of the right

2.4.2 Relations between A,B and κ, λ

The ramp experiment

We finalize this formal electrical analogy by comparing the fundamental terms used to describe quantitatively the responses of the system to both experiments. We got that at the end of the ramp experiment, the ratio of the temperature change already achieved to the total expected temperature change was $\frac{A}{A+B}$. It is also clear that at the end of this very ramp, using Eq. 1.1 we have:

$$\kappa \Delta T_f + \frac{\tau_1}{t_f} \lambda \Delta T_{eq} = \lambda \Delta T_{eq} - \lambda \Delta T_f \tag{2.26}$$

This leads to the very important identity that concludes this analysis:

$$\frac{A}{A+B} = \frac{\Delta T_f}{\Delta T_{eq}} = \frac{\lambda \left(1 - \tau_1 / t_f\right)}{\lambda + \kappa} \tag{2.27}$$

This gives the ratio A/B as:

$$\frac{A}{B} = \frac{\lambda\,(1 - \tau_1/t_f)}{\kappa + \lambda\tau_1/t_f} \tag{2.28}$$

This points out the fact that the physical parameters λ and κ govern the temporal evolution of the climate.

We can also notice that using the classical relation 2.6 (and the appropriate κ) we would get the compact equality:

$$\frac{A}{A+B} = \frac{\Delta T_f}{\Delta T_{eq}} = \frac{\lambda}{\lambda + \kappa} \tag{2.29}$$

In fact this is true for the extreme situation when the short characteristic time is much smaller than the experiment length. A model with a shorter τ_1 might satisfy Eq. 2.6.

The step experiment

From the electrical circuit for the step forcing, we could also define A and B using the initial conditions. Indeed, when the forcing is imposed, it is absorbed by the surface ocean since no temperature change has yet occurred. The initial condition are thus:

$$\begin{cases} \Delta T(0) &= 0 \\ U_0 &= L_s \dfrac{di}{dt}(0) \end{cases}$$

$$\begin{cases} A + B &= \Delta T_{eq} \\ \dfrac{A}{\tau_1} + \dfrac{B}{\tau_2} &= \dfrac{\lambda \Delta T_{eq}}{L_s} \end{cases}$$

From this system of equations, and given $\tau_2 \gg \tau_1$ we have the following expressions for A and B:

$$A = \frac{\lambda \Delta T_{eq}}{\lambda + \kappa}$$
$$B = \frac{\kappa \Delta T_{eq}}{\lambda + \kappa}$$

Hence we find again the important relation (which is the first order approximation of expression 2.28):

$$\frac{A}{B} = \frac{\lambda}{\kappa} \tag{2.30}$$

This latter equality gives a mean to evaluate κ, as long as λ, A and B are known.

2.5 Analysis of the simulations outputs

2.5.1 The GCM outputs

To check the validity of our electrical analogy, it is now interesting to see how well the simulations outputs fit with the results predicted by the electrical circuit. This is why we analyse further the step experiment. We already showed that the climate system behaves linearly. This is why it is possible to fit the temperature and net TOA flux curves by exponential terms. Finding these terms might enable us to find the feedbacks and ocean heat efficiencies of the models straight from the experiments. Moreover, it might give precious information on the transient state,more specifically the shares of ΔT that may occur in shorter and longer terms. This point is essential since it provides the distance to equilibrium that we are currently experiencing. Is the greater change in temperature already past or is it to be later, is a crucial topic. To begin with, we show on figure 2.7 the shape of the temperature outputs for both experiments, which is an illustration of the linearity of the system (see also figure 2.5).

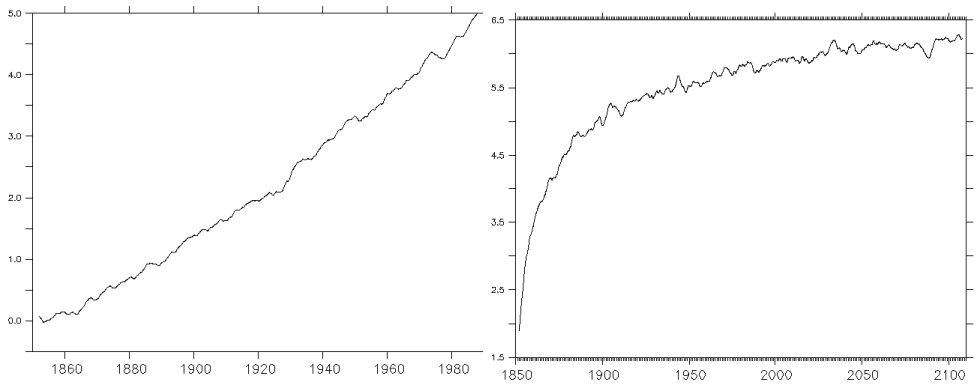

Figure 2.7: Evolution of ΔT (K) with time (in years, starting in 1850) for the ramp (l., characterised by an almost flat signal on the first decade) and step (r.) experiments.

We see on the left panel of figure 2.7 that the temperature signal seems to be exponential. This cannot be seen at very short time scales but is clear enough after a century of the ramp experiment. What was considered in Gregory and Mitchell [1997] as a linear evolution was probably in fact the beginning of an exponential evolution, as we suggested previously.

2.5.2 Characteristic times of the GCM

We introduced previously the decomposition of the response to a step forcing on two characteristic times. This is why we look for exponential functions to fit the outputs curves. This can be done on the flux outputs (basically a decreasing exponential) or

on the temperature curves. Both methods should give similar characteristics if the GCM is sufficiently linear.

We fit the temperature curves with functions similar to 2.14. We impose ΔT_{eq} obtained by the regression method. We do not impose $\Delta T = 0$ for $t = 0$ since early warming has already occurred after a few months while we fit averaged signals. To sum up, the characteristic times and the initial condition are let free to adjust. We can iterate this functional fit for any temperature curve, namely the globally averaged one, but also spatially or seasonally limited ones.

We can apply this exponential fit to the N curve, assuming that it is nought at equilibrium. For reasons already explained, we do not impose $N = \Delta Q$ for $t = 0$ otherwise the fit would be of very few significance. In table 2.1, we present the results of the exponential fits for both methods. The good correlation between the characteristic times supports the linearity assumption. Although the physical objects are of a very different nature, they are linked by very simple linear relations, hence such a similitude. Both exponential regressions are highlighted on figure 2.8. For these regressions we have used mobile averages of 4 years. We find the same characteristic times for 1-year averages. We found that the value of τ_2 is strongly dependent on the equilibrium condition we impose. In fact, the simulations are too short to obtain a reliable fit. We assume that the values of τ_1 and A are reliable, while the values of B and τ_2 essentially depend on the controversial idea that our model tends toward equilibrium for long times. Anyway, the value of interest is A since it gives the imminent warming due to an abrupt increase in CO_2 concentrations.

	A_0	B	A/B	τ_1	τ_2
ΔT	2.3	3.3	0.7	22	580
N	1.9	2.6	0.73	19	562

Table 2.1: Comparison of the characteristics of the model obtained from the exponential fit of ΔT and N (τ_i are given in years)

To support the validity of the two exponential terms fit, we tried to fit the signal with only one, which leads to much less accuracy. On the contrary a 3^{rd} exponential term did provide a characteristic time for fast atmospheric processes but they were not considered in our electrical analogy. Finding similar characteristic times and similar A/B for ΔT and N once more supports the linear theory introduced. A supplementary interesting value is the ratio $A_{\Delta T}/A_N$ (or $B_{\Delta T}/B_N$) that are 0.76 (resp. 0.79) which corresponds to what was expected given relations 2.17. We insist eventually on the importance of determining the pre-exponential coefficients A and B since they provide the relative importance of the shorter and longer term changes. If $A \gg B$ then most of the temperature change will be due to the short term response. Otherwise, the temperature evolution might be more driven by the deep ocean.

Now, to make a parallel with the fundamental relation 2.27, we must bear in mind that the A coefficient provided by the exponential fit does not consider the fast initial response. That is why we recalculate the values of A. In table 2.2 we

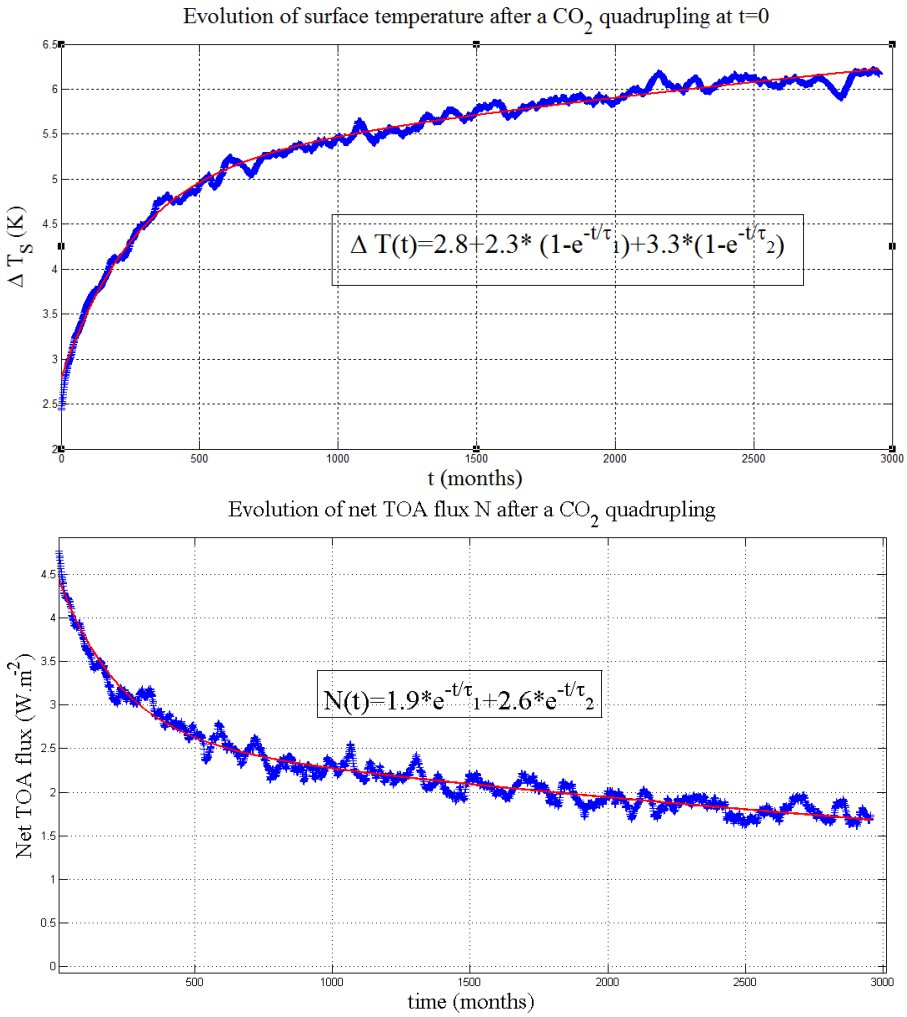

Figure 2.8: Exponential fits applied to ΔT(up) and N(bottom)

make the link between the exponential fits on the one hand, and the linear regression on the other hand. Former studies defined κ as the ratio $N/\Delta T$ at the end of the ramp experiment (in that case, we would have $\kappa = 0.56$). As the relation between N and ΔT is not linear, this former definition does not have much sense and κ would depend on the length of the run. Our new definition seems physically more relevant.

It is interesting to note that the value of A obtained for ΔT corresponds almost exactly to the value of ΔT_f at the end of the ramp experiment. Once more this gives sense to the linear approach.

Eventually we present the values predicted by the electric analogy and the experimental results for the globally and yearly averaged step experiment in table 2.3. Although the characteristic times differ from those predicted by the theory, we point out that the ratio A/B observed perfectly fits with the theoretical model. In a word,

	A	B	A/B	$\frac{\lambda(1-\tau_1/t_f)}{\kappa+\lambda\tau_1/t_f}$
ΔT	5.1	3.3	1.55	1.35
N	3.9	2.6	1.5	1.35

Table 2.2: Adjusted parameters of the model calculated from the exponential fits of ΔT and N

the values of the characteristic times remain uncertain, but the shares of global warming on short or long term seem quite reliable.

	A	B	A/B	τ_1	τ_2
Electrical Circuit	5.1	3.3	1.55	4.8	1300
GCM Experiment	5.1	3.3	1.55	22	580

Table 2.3: Comparison of the typical time scales obtained from the electrical analogy and from the exponential fits

We also point out that the experimental determination of A and B can help to evaluate κ. Indeed, we have said that its determination from the regression featured on figure 2.6 is rather uncertain. Given that the methods providing A, B and λ seem more robust, we present in table 2.4 the values of κ obtained from Eq. 2.30. The value obtained is greater than the one obtained from the regression. It highlights the inaccuracy of the regression method for the determination of κ.

	A	B	κ
ΔT	5.1	3.3	0.50
N	3.9	2.6	0.51

Table 2.4: Evaluation of κ from A, B and $\lambda = 0.77$

We provide now some leads to explain the difference between experimental and theoretical characteristic times. We had predicted larger time scales from the electrical analogy. In fact, the GCM might not have an overturning circulation that reaches the whole ocean. To evaluate τ_2 from the circuit, we considered an equivalent rectangular. It means that the deep ocean is effectively deep everywhere on Earth. In fact, it does not take into account the coastal areas where strong atmosphere/ocean interactions might exist. In a way, let say that the 1300 yrs is an upper limit in the case the whole ocean responds to a surface warming, but in fact only part of it might notice this change. The deep ocean is composed of several distinct layers (intermediary or deep waters) and they do not respond as a unique water mass. As far as the short time scale is concerned, we assume that the response times of each feedback (not considered in the simple model) tend to lengthen the global response time of the surface ocean.

2.6 Conclusions

Using both ramp and step experiments, we have pointed out their complementarity in terms of climate analysis. Thanks to the simple electrical analogy we have highlighted the linearity that characterises a GCM experiment. The values of A, B, ΔT_{eq} and λ were obtained from the step experiment while κ was obtained from the ramp one. The electrical analogy gave some physical interpretation to all these parameters and the empirical linearity of the GCM allowed us to draw some interesting algebraic relations. We insist that A and τ_1 seem reliable while the long characteristic times are more ambiguous. In our simple model, the behaviour of a GCM is determined by the values of κ and λ only.

CHAPTER 3

FAST RESPONSES OF THE CLIMATE

In this chapter we focus on the forcing term ΔQ. We highlight that it can be seen as the sum of a purely radiative term due to CO_2 on the one hand and other fast responses of the climate itself on the other hand. The understanding of the forcing ΔQ is a crucial step towards the final goal of this work: evaluating the feedback parameters of various climate components.

3.1 Decomposition of ΔQ

Once more, we use the regression method for N and ΔT. We consider first the clear-sky component of the forcing (subscript N), while the difference between the total-sky and clear-sky forcings is called the cloud component (subscript C). We also differentiate the SW (S) and LW (L) terms, so that eventually, following Gregory and Webb [2008], N can be written:

$$N = F_{LN} + F_{LC} + F_{SN} + F_{SC} \tag{3.1}$$

On figure 3.2 we plot the regression of each of the F_i versus ΔT and present the values of the corresponding forcings, namely the y-intercepts of each straight line. We must bear in mind that these forcings might have no physical signification. In fact we just extrapolate at a given time the forcing that would result from a reverse linear evolution. We have no access to the very beginning of the experiment as featured on figure 3.1.

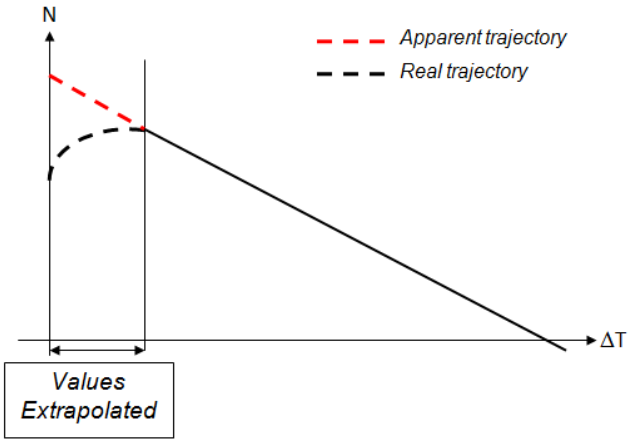

Figure 3.1: Illustration of the extrapolation for the short time scales of N evolution

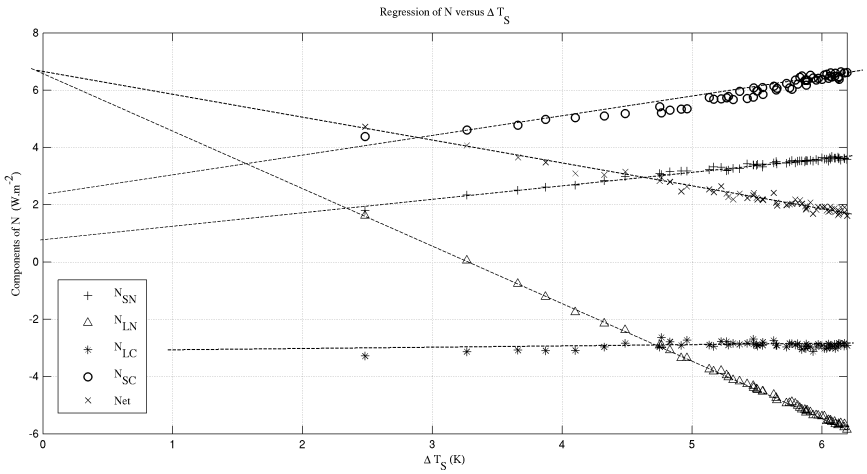

	F_{LN}	F_{LC}	F_{SN}	F_{SC}	N
ΔQ	6.5	-3.2	0.84	2.14	6.5
λ	2.0	0.05	-0.46	-0.7	0.77

Figure 3.2: Decomposition of the net TOA flux N in terms of clear-sky and clouds contributions

3.1.1 Qualitative description of the regression plot

The first striking point is the relative amplitude of the cloud component, especially the LW negative forcing. This forcing term might be abusively interpreted as a feedback by Partial Radiative Perturbation (PRP)-like methods that compare a cli-

matological climate and a CO_2 perturbed climate. In fact, considering for instance the F_{LC} regression, we see that the slope is almost flat. As we know, the stiffer the slope, the greater the sensitivity of the corresponding flux to ΔT. It means that this cloud response has almost no sensitivity to ΔT and is reduced to its fast response. In a word, clouds LW forcing seems to be a direct consequence of the input of CO_2 into the atmosphere. We also notice that the sum of the ΔQ_i does not equal the total forcing (more exactly we have an error of $3,4\%$), neither for the feedback parameters (this error is $15,6\%$). We deduce the degree of incertitude of this regression method that is more or less 10%.

More generally the climate forcings might depend on the nature of the primary external forcing. For a solar irradiance increase, the primary forcing would be a SW forcing and might have no impact on the clouds cover. Although feedback parameters can be considered independent of the nature of the forcing (they only quantify the response of climate to an increase of surface temperature, whatever the origin of the warming), forcings (and thus equilibrium temperature) depend on the nature of the forcing.

We also highlight that the total forcing is more or less the same as the CS LW forcing. This might breed errors of interpretation since purely radiative calculations give a CO_2 forcing that corresponds quantitatively to the forcing obtained by the regression method. Fast conclusions would lead to a misunderstanding of the phenomena implicated. In fact, this is only a coincidence that both values match that well. It means that clouds operate globally as if they were absent (in terms of radiative budget), which is the topic of next paragraph.

3.1.2 An apparent neutrality of clouds

We have seen that the net forcing is almost the same for CS and total-sky conditions. In fact this results from the opposite signs forcings of clouds in SW and LW. That's why it is interesting to separate N into SW and LW components:

$$N_{SW} = \Delta Q_{SW} - \lambda_{SW} \Delta T \tag{3.2}$$
$$N_{LW} = \Delta Q_{LW} - \lambda_{LW} \Delta T \tag{3.3}$$

We make the regressions of these two equalities to get the SW and LW sensitivities, and the corresponding forcings. Results are given in table 3.1. Surprisingly SW and LW apparent forcings are equivalent although the initial one is mainly a LW forcing. This highlights the role of the clouds: even though they do not change quantitatively the energy balance, they modify it quantitatively through the SW budget.

3.1.3 Comparison with other simulations

The former model It is interesting to compare the values of figure 3.2 to those found with a previous version of the IPSL model(figure 3.3) that used a slab ocean.

	SW	LW
ΔQ (W.m^{-2})	3.0	3.5
λ (W.m^{-2}.K^{-1})	-1.2	2.0

Table 3.1: Decomposition of ΔQ and λ in SW and LW components

We see that the major change in the model is the fast response of the clouds in the LW. This response has changed by almost 12%. The sensitivity of clouds in the LW has also changed, and it is interesting to notice that the clear-sky LW forcing is greater in the former model. Such differences can be explained by the modification of clouds representation in the new model.

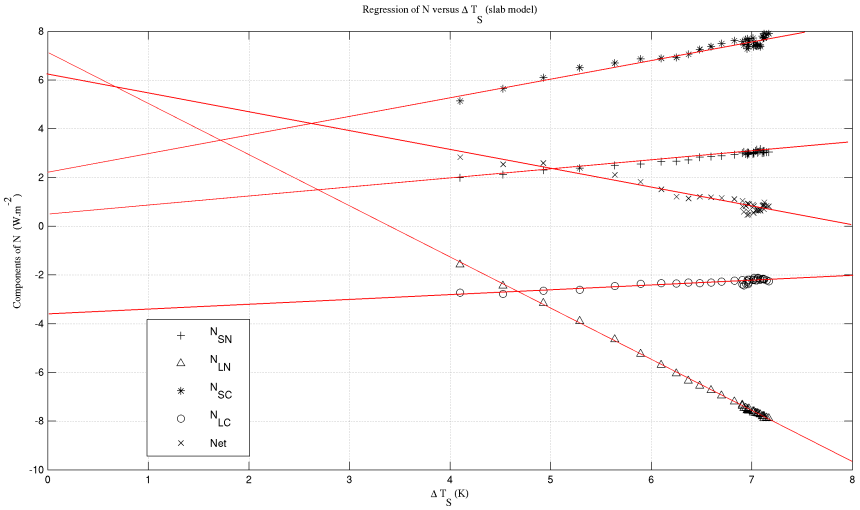

	F_{LN}	F_{LC}	F_{SN}	F_{SC}	N
ΔQ	7.1	-3.6	0.45	2.3	6.3
λ	2.1	-0.19	-0.36	-0.75	0.78

Figure 3.3: Decomposition of the net TOA flux N in terms of clear-sky and clouds contributions for the old model

The AMIP4xCO2 simulation We also compared the results to those obtained in the AMIP4xCO2 experiment. In the latter, sea surface temperature (sst) is fixed and climate is forced by a quadrupling of CO_2. We expect to isolate the fast responses with this simulation. It is formally equivalent to the regression method, except that the surface temperature over the continents is allowed to evolve. Although the usual flux are not constant during the experience due to the evolution of continental surfaces, the forcings find here are approximately the same as in previous sections. However this is not true for F_{SC} that is much too large for the AMIP4xCO2 experiment.

3.2 Physical fast response processes

The point here is to split the climate response into a quick response due to the forcing itself (and supposed at first order to be proportional to its intensity) and a feedback response proportional to the change in surface temperature, thus taking more time.

We rewrite the so-called forcing ΔQ as the sum of a purely anthropic term due to CO_2 emissions and other fast responses (fr) of the climate:

$$\Delta Q = \Delta Q_{CO_2} + \sum_i \Delta Q_{i,fr} \tag{3.4}$$

3.2.1 Fast response of clouds

As suggested by the value of F_{LC} the clouds seem to have a fast response that is seen by the system as a negative forcing. Therefore we focus on the evolution of the cloud cover during the simulation. We regressed the cloud covers for three levels(high (h), medium (m) and low (l)) by ΔT. The y-intercept corresponds to a change in cloud cover that we interpret as the fast response. Quantitatively, relatively to the control state, the fast responses are a diminution of 6% of high clouds, a diminution of 4% of the medium clouds and an increase of 3% of the low clouds cover. The total cloud cover decreases instantaneously of 2% after the CO_2 forcing is imposed. We bear in mind that the cloud cover has no evident link with the radiative impact of the clouds, but it gives substance to a physical interpretation of the clouds fast response. We plotted on figure 3.4 the repartition of the fast response of high clouds (changes are in % of cloud cover). We compared the situation after 4 years to the initial one. It features an increase of high clouds in polar regions while almost everywhere else they tend to decrease.

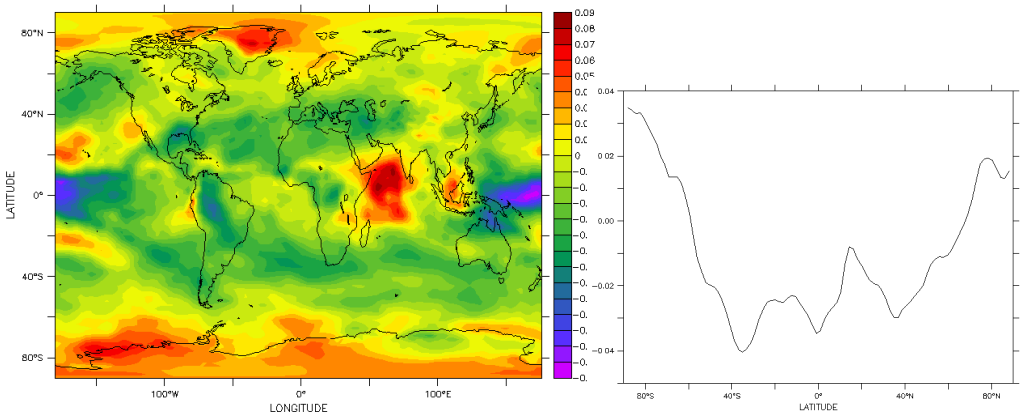

Figure 3.4: Spatial repartition of the high clouds fast response (in cloud cover)

Quantitatively, the forcing corresponding to the fast response is relevant. We make the assumption that the F_{LC} term is due to the fast decrease of high altitude

clouds, the very clouds that are the most efficient for greenhouse effect. Assuming that the greenhouse effect attributed to clouds in a control state is about 50W.m^{-2} (see Kiehl and Trenberth [1997]), decreasing of 6% the high clouds cover might decrease this effect by 4W.m^{-2} which is quantitatively the value of the forcing observed. We thus conclude that the negative forcing due to clouds is due to a rapid response of high clouds to the CO_2 forcing. This diminution is mainly localized on the intertropical band (see figure 3.4, especially above the Pacific). This is basically where the greenhouse effect of clouds is the stronger.

Regarding the SW forcing of clouds, we see that they have a positive forcing of 2.14W.m^{-2}. We can explain it by the variation of the clouds albedo, that would be coherent with the decrease of the global cloud cover. We can define the SW flux due to the albedo of clouds (it is done in chapter 4). Thus we can plot the variation of this flux versus ΔT. The y-intercept corresponds to the fast response of clouds albedo. It is evaluated to 2.2W.m^{-2}. With a diminished cloud cover, more solar radiation is absorbed, hence this positive forcing. Another approach consists in considering directly the decrease of the total cloud cover. The cloud albedo is estimated to 80W.m^{-2} so a diminution of 2% of the cloud cover would lead to a forcing of 1.6%.

3.2.2 Fast response of the hydrological cycle

Many works have pointed out a decrease in precipitations in earlier times of a global warming. This is also what we observe in the IPSL model. Quantitatively, there is an apparently instantaneous 6% drop in precipitations at the beginning of the run. Later on, average precipitation rates increase. The classic explanation for this diminution of precipitation is based on Clapeyron's law. When the atmosphere warms up, the quantity of water vapour it can hold is also increased and thus after a brutal increase in temperature, precipitation rates diminish. A more detailed description of this fast response and the difference with the slow one can be found in Andrews et al. [2010] (they got a decrease of 2.5% of the precipitations for a doubling of CO_2). So that the atmosphere remains at equilibrium, to compensate the warming due to CO_2 absorption, latent heat release must diminish, hence precipitations. This interpretation assumes the atmosphere reaches radiative equilibrium as soon as possible after a perturbation.

It is interesting to look at the evaporation rates. They present exactly the same features as precipitations, so no change in the water content appears. The fast response of the global water content (in kg.m$^-$2) is evaluated to an apparent 7% decrease. However, this forcing is only apparent since a thorough analysis shows no response for the first months of the run. To be more accurate, we plotted the evolution of average specific humidity above 800hPa with ΔT. It highlights that there is no fast response of water vapour a these altitudes, where greenhouse effect might be more efficient. We conclude that the LW forcing is due essentially to the external forcing and the clouds response, while the clear sky SW forcing is attributed to the only external forcing.

Summary

In Table 3.2 we provide the values of the fast responses (namely forcings) just calculated. From Kiehl and Trenberth [1997] we assume that the LW cloudy sky effect of CO_2 is 0.75 times that of clear sky conditions. On the contrary, we assumed that there is almost no overlap for the SW between the clouds and CO_2 so that N_{SC} correspond to the unique clouds albedo effect. Thus the forcing given by N_{LC} gathers the overlap effect of the average cloud cover and its fast response. They will be of major importance in Chapter 4.

	Clouds Albedo	Clouds GE	CO_2 LW	CO_2 SW
ΔQ	2.14	-1.58	4.89	0.84

Table 3.2: Attribution of fast responses to various components of N (in W.m^{-2})

3.3 Atmospheric flux into the atmosphere

A flux that has not been much discussed until now is the net flux into the atmosphere, denoted F_{atm}. It is the sum of the net SW, LW and latent and sensible heat flux into the atmosphere. At first sight, it is almost constant in the step experiment with a value of less than 0.4W.m^{-2}. However, splitting it into its SW, LW and sensible and heat components, we find interesting features, that in a all sum to zero. In fact the SW forcing is 3.4W.m^{-2}, the LW one equals -1W.m^{-2} while the part of the sensible and latent heat is -4W.m^{-2} which corresponds to the decrease in precipitation.

From the parallel analysis of the atmospheric and TOA net flux, we highlight an important feature as far as the forcing is concerned. The global forcing ΔQ can be decomposed in an atmospheric and a surface forcing. One can write:

$$\Delta Q = \Delta Q_a + \Delta Q_s \tag{3.5}$$

Combining this decomposition with the SW and LW decomposition, we conclude that the SW forcing of the atmosphere equals the global SW forcing. This means that the SW forcing concerns only the atmosphere. This is understood as the increased absorption of atmospheric components for a less cloudy sky. For the surface,the change in SW downward radiation is minor due to the opposite effects of the clouds albedo and the atmosphere absorption. We also point out that the LW forcing mainly forces the surface. Indeed, the greenhouse effect of CO_2 is seen by the surface as an increase in LW downward radiation.

We give here more details on the way latent heat fluxes are calculated. Latent heat is taken from the ocean to evaporate water. This gives the upward latent heat flux. In fact this heat flux is only a potential source of energy since it is released into the atmosphere only through precipitations. A very important consequence of this evident statement is that for local energy balance, the latent heat flux is

not a real flux transferred to the atmosphere. It it true only for globally averaged calculations in which any latent flux from the ocean will eventually be transferred to the atmosphere, either through sensible heat if the water vapour exchanges heat with its environment, or through precipitations. This is why it is interesting to define the quantity $(Evap - Precip)T_s$ (and its variations with time) that gives for a grid cell the energy that is effectively transferred to the atmosphere, assuming that evaporation and precipitation occur at surface temperature. The variation of this quantity is plotted on figure 3.5. Averaging this quantity on the whole surface of Earth, this gives a new flux from the ocean to the atmosphere, different from the heat or sensible flux, that is linked to the non uniformity of precipitation and evaporation on Earth. More simply, if evaporation occurs at low latitudes, it holds a lot of potential energy, and if the precipitations mainly occur at high latitudes, the energy released is smaller than the potential one, the rest being transferred through heat exchanges.

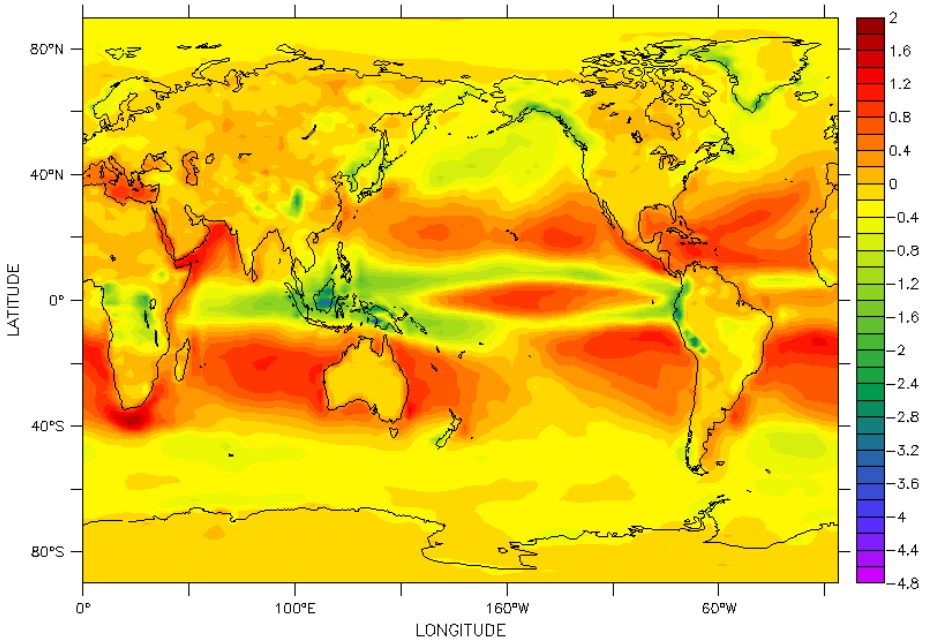

Figure 3.5: Variation of the heat flux from the ocean to the atmosphere due to Earth temperature non-uniformity

In conditions of global warming, the hydrological cycle is amplified and Hadley cells tend to spread at higher latitudes. Consequently, this transfer of energy from the ocean to the atmosphere is enhanced. This process corresponds approximately to 10% of the flux into the atmosphere and strongly depends on surface warming.

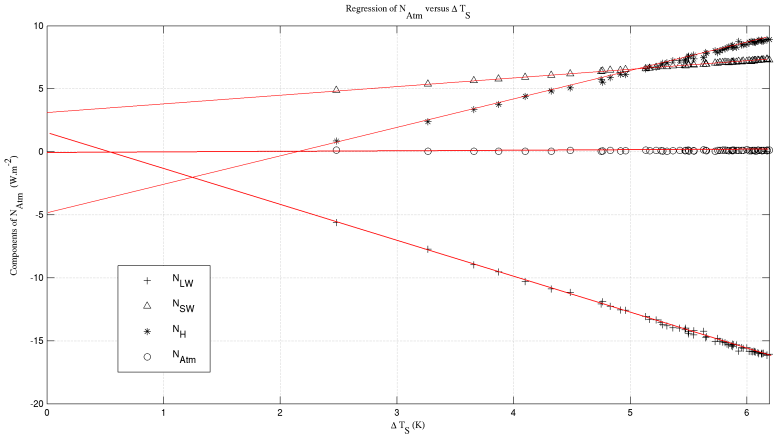

	N_{SW}	N_{LW}	N_H	N_{Atm}
ΔQ	3.25	1.7	-4.9	0.02
λ	-0.66	2.9	-2.24	-0.01

Figure 3.6: Decomposition of N_{atm}

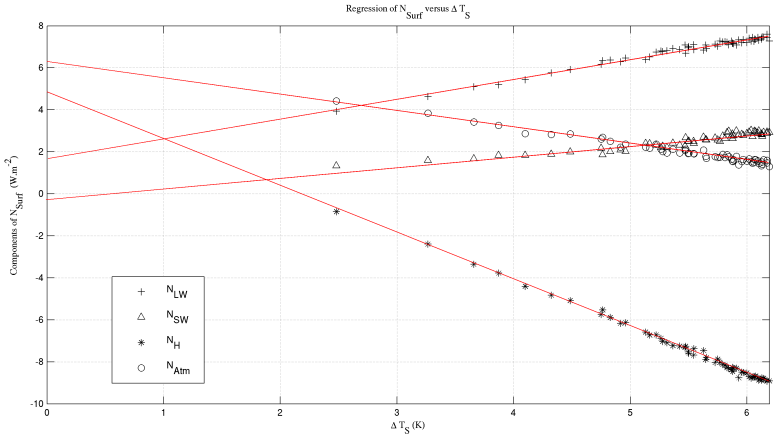

	N_{SW}	N_{LW}	N_H	N_{Surf}
ΔQ	-0.2	1.7	4.9	6.3
λ	-0.5	-0.95	2.2	0.79

Figure 3.7: Decomposition of N_{surf}

CHAPTER 4

A NEW APPROACH OF THE FEEDBACK ANALYSIS

In this part we aim at developing an original method for the evaluation of the amplitude of each feedback mechanism. Classically, to test the intensity of a feedback, the corresponding physical quantity (this can be water vapour, temperature or surface albedo) is modified from a control run, and the resulting climate compared to the control run. The change in net TOA radiative budget between the two experiments (ΔQ_i) is attributed to the change in the physical quantity. From this, feedback parameters can be inferred by the identity $\Delta Q_i = \lambda_i \Delta T_s$, after explicitly making a link between the change in the physical quantity and the change in surface temperature. This method is called Partial Radiative Perturbation (PRP) method (the Kernel method is an extension of it) and is detailed in Soden et al. [2008]. These calculations are based on non realistic evolutions of the climate since one or more parameter is kept unchanged for the run. Hence all feedbacks cannot interact which is arguably a problem. These methods could be called exclusive, while we aim at providing an inclusive one. In this chapter we propose a diagnostic way of evaluating feedback parameters λ_i from the variations of the Earth radiative budget in the course of a GCM simulation. We need only one simulation (and the climatological control run) to evaluate all the feedbacks and it is a realistic evolution of the climate (assuming the GCM is effective).

4.1 General description of the method

We use the ramp forcing until quadrupling and focus on the variations of TOA and surface net flux during this lapse. From now on we define the flux with the following nomenclature: LW refers to longwave, SW to shortwave, the subscripts t and s respectively to TOA and surface, and the arrows indicate the direction of

the flux, downward or upward. The suffix *cs* is added for clear sky components. They correspond to computations in which the clouds were omitted for the radiative calculations. For instance, $LW_{t\downarrow}$ refers to the LW flux downward TOA and $SW_{s,cs\uparrow}$ is the surface SW flux upward in clear-sky conditions.

We base our work on the ramp experiment since for such a linear atmospheric forcing, all of the variations (cloud cover, water vapour content, radiative flux...) are found to be linear with time (hence more or less with the change in temperature), which simplifies the comparisons between the flux components. We use the net TOA flux balance in order to separate the role of various factors. We differentiate between shortwave and longwave components of the net balance. Scheme 4.1 summarizes all the subsequent qualitative analysis.

The method is based on a thorough analysis of equation 1.1. From this identity we decompose N and ΔQ with the method described in chapter 3. N is given by the outputs of the simulation, but it includes the forcing and the climate responses, namely the fast and slow ones. We give a physical decomposition of N in fast and slow contributions at the end of the experiment using the various outputs given by the model. We can write:

$$\begin{aligned} N &= \Delta Q - \sum_i \lambda_i \Delta T \\ N &= \sum_i N_{i,slow} + \Delta Q_{CO_2} + \sum_i \Delta Q_{i,fr} \\ \sum_i N_{i,slow} &= -\sum_i \lambda_i \Delta T \end{aligned}$$

In this decomposition, the N_i will be given by the outputs of the model, the forcings are known from previous chapter, hence we can associate a feedback parameter to a given change in N by:

$$\lambda_i = -\frac{N_{i,slow}}{\Delta T_f} \tag{4.1}$$

where $N_{i,slow}$ is the contribution of the slow response of feedback i to N and ΔT_f the change in surface temperature, both at the end of the ramp experiment. It is clear that ΔT_f is given at the end of the simulation. We use here $\Delta T_f = 5$K. On the contrary $N_{i,slow}$ will be computed from the analysis of the fast and slow responses of the climate.

4.2 Components of the energy budget

4.2.1 SW components

Atmospheric Absorption and Reflection To evaluate the role of atmosphere in the SW, due to clouds and atmospheric composition, we compute the difference

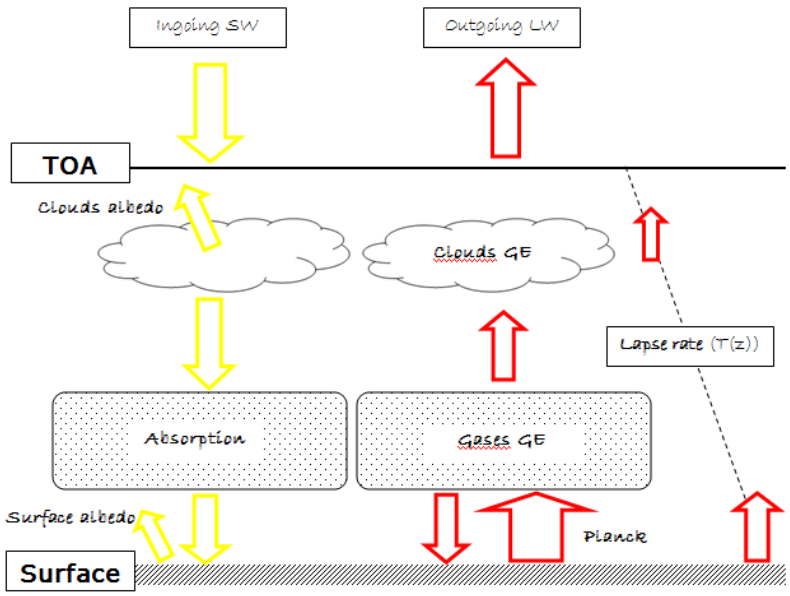

Figure 4.1: Qualitative description of Earth radiative budget

between $SW_{t\downarrow}$ and $SW_{s\downarrow}$. This calculation leads to the share of direct solar radiation that is absorbed or reflected by the atmosphere. To differentiate between the clouds and water vapour SW interactions, we use the clear-sky calculations of the simulations. Atmospheric reflection is due to Rayleigh diffusion by atmospheric components but also to Mie diffusion by clouds (this is the cloud albedo effect).

Surface Albedo We define the surface local albedo α as:

$$\alpha = \frac{SW_{s\uparrow}}{SW_{s\downarrow}} \tag{4.2}$$

All the radiation that is not reflected by the surface will be absorbed and hence heats the surface. We can plot the evolution of the global albedo with time, which more or less corresponds to the melting of sea ice at polar latitudes. An equivalent planetary albedo can be defined from the TOA SW flux but will not be useful in this study.

4.2.2 LW components

Planck black-body emission We now have to deal with the LW components. We begin with the so-called Planck effect which states that the Earth LW emission is given by Eq. 1.4. As the surface emissivity is 1 in the model we use, the surface upward LW flux is nothing but this black-body effect, which appears to be linear with time in the simulations since the temperature is (see Chapter 1)

Greenhouse effect The greenhouse effect corresponds to the ability of the atmosphere to contain the Earth LW radiation, leading to the warming of lower troposphere compared to a non-absorbing atmosphere. We define it as $(LW_{s\uparrow} - LW_{t\uparrow})$. Greenhouse effect can be attributed to greenhouse gases (mainly water vapour and CO_2) but also to clouds, both absorbing LW radiation. The greenhouse effect (see Annex C) is due to the vertical gradient of temperature. In fact, gases and clouds absorb a given quantity of LW radiation coming from below but their emission is limited by their temperature. The lapse rate is the vertical gradient of temperature and mainly governs the greenhouse effect. Once more we will use the clear-sky component to approximatively isolate the gases contributions, before adding the clouds effect. It has to be noticed that in terms of feedbacks, part of the greenhouse effect forcing is due to a climate response (namely the water vapour or clouds responses) while the remaining comes from the direct anthropic CO_2 effect.

4.3 Assumptions

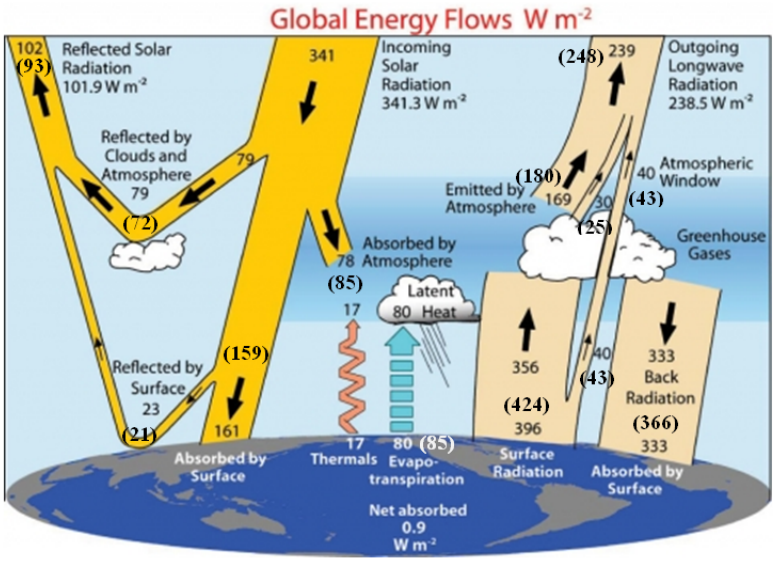

Figure 4.2: The Earth radiative budget (from Trenberth et al. [2009]) and projection after a CO_2 quadrupling from our own analysis (in parenthesis)

As we aim at differentiating the distinct effects of distinct physical feedback mechanisms that contribute to the net downward TOA flux into the atmosphere, we must be able to distinguish the very mechanisms involved. We base our work on the previous analysis of the Earth budget presented in Kiehl and Trenberth [1997] and updated in Trenberth et al. [2009], whose summary is given on figure 4.2.

Assumption 1 We assume that the absorption of the SW radiation only occurs for the downward flux, meaning that the SW flux reflected by the Earth is not absorbed, neither by clouds nor by the atmosphere. This assumption is supported by the calculation of the difference between $SW_{t,cs\uparrow}$ and $SW_{s,cs\uparrow}$, that is the albedo effect of the atmosphere plus the upward atmosphere absorption in CS conditions. For the ramp experiment, this remains constant. Assuming that the CS atmosphere reflection (namely Rayleigh, estimated for the model at 18.1W.m^{-2}) does not depend on temperature or water vapour content (since it is few of the atmosphere mass), we conclude that there is no absorption between the surface and TOA, otherwise the calculated difference would be dependent on water vapour (hence on time). It can be interpreted as the saturation of the absorption bands on the way downward.

Assumption 2 The variation of clouds SW absorption is neglected, we only consider their reflective effect. This is supported by the model evaluation of atmospheric absorption in CS conditions (64 W.m^{-2}) and in total-sky conditions (68 W.m^{-2}). The variation of atmospheric absorption along the ramp experiment is the same for cloudy and clear-sky conditions (namely an increase of 7 W.m^{-2}). Clouds increase atmospheric diffusion, hence energy is more likely to be absorbed in cloudy conditions since the apparent path of light is enhanced. Variations of SW atmospheric absorption will be attributed only to a change in gaseous absorption, the change in cloud cover (namely the indirect effect of clouds) being neglected.

Assumption 3 We use results from Kiehl and Trenberth [1997] to evaluate the share of each component (clouds, water vapour, CO_2) in both SW absorption and LW greenhouse effect. We suppose that in conditions of global warming, the relations proposed to make a link between CS and total-sky conditions are still valid. These values are provided in 4.4.

Assumption 4 It is very difficult from the outputs of the simulations to differentiate between lapse-rate and Planck effect. That's why the Planck parameter is evaluated from the Kernel method introduced in Soden et al. [2008] and we will take $\lambda_P = 3.2$W.m^{-2}.K^{-1} (see Annex C for a simple physical interpretation of this value). Given this feedback parameter has few disparity among models, we take it as the contribution of Planck in order to evaluate other LW contributions. The lapse-rate effect is determined by the method described in Annex C and we consider that there is no fast response of the lapse-rate.

4.4 Formal decomposition of N

We try now to explicit the various $N_{i,slow}$ of equation equation 4.1. To do this we isolate the contribution of a mechanism i along the experiment (which is represented by the theoretical decomposition on figure 4.3

$$\Delta N_i = N_{i,slow} + \Delta Q_{i,fr} \tag{4.3}$$

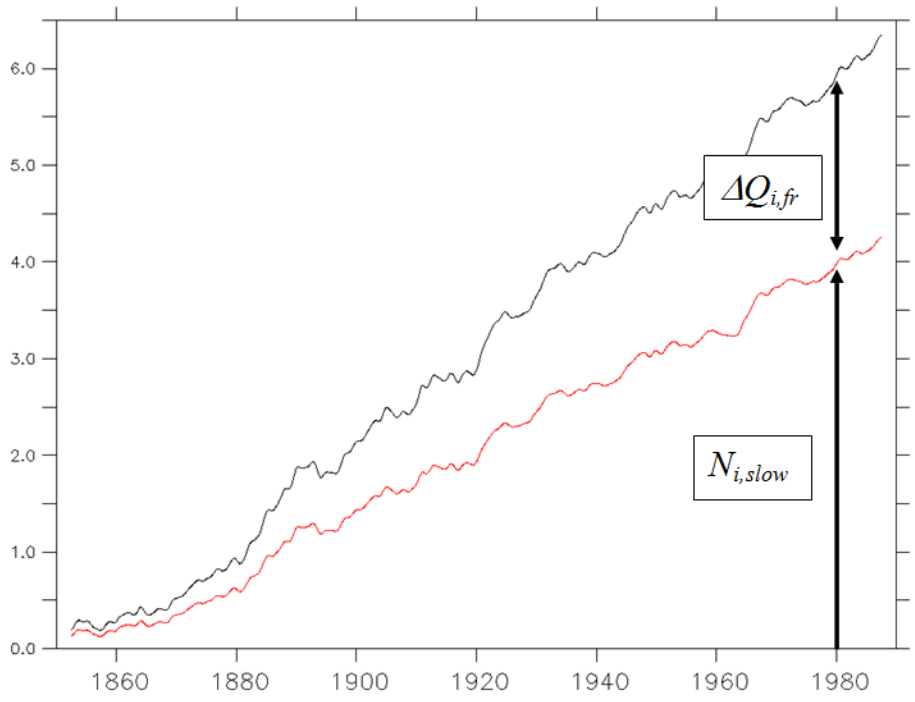

Figure 4.3: Decomposition of the contribution of clouds albedo to the net radiative TOA budget

$N \equiv \Delta N$ is the variation in the net TOA budget, so it can be rewritten (assuming the solar insolation is constant):

$$\Delta N = \Delta(SW_{t\downarrow} - (LW_{t\uparrow} + SW_{t\uparrow})) \tag{4.4}$$
$$\Delta N = -\Delta(LW_{t\uparrow} + SW_{t\uparrow}) \tag{4.5}$$

that is the sum of the variations of the outgoing SW and LW flux. We have supposed here that on average the solar flux is constant (for sufficiently long periods). We explicitly treat the SW and LW components separately.

4.4.1 Shortwave

We focus on the outgoing SW radiation. It comes either from the reflection of clouds and atmosphere, or from the surface. So we write:

$$SW_{t\uparrow} = \alpha SW_{s\downarrow} + (Ray + \alpha_c) \tag{4.6}$$

where Ray means Rayleigh and α_c refers to the clouds albedo. Note that α is non-dimensional while α_c is in W.m^{-2}.

Assuming that Rayleigh effect does not change with time:

$$\Delta SW_{t\uparrow} = \Delta(\alpha SW_{s\downarrow}) + \Delta\alpha_c \tag{4.7}$$
$$\Delta SW_{t\uparrow} = \alpha\Delta SW_{s\downarrow} + SW_{s\downarrow}\Delta\alpha + \Delta\alpha_c \tag{4.8}$$
$$\Delta SW_{t\uparrow} = \alpha\Delta(SW_{t,\downarrow} - (\alpha_c + Ray) - Abs_{Atm}) + SW_{s\downarrow}\Delta\alpha + \Delta\alpha_c \tag{4.9}$$
$$\Delta SW_{t\uparrow} = -\alpha\Delta(\alpha_c + Abs_{Atm}) + SW_{s\downarrow}\Delta\alpha + \Delta\alpha_c \tag{4.10}$$
$$\Delta SW_{t\uparrow} = \underbrace{-\alpha\Delta Abs_{Atm}}_{Atmosphere\ \ Absorption} + \underbrace{SW_{s\downarrow}\Delta\alpha}_{Surface\ \ Albedo} + \underbrace{(1-\alpha)\Delta\alpha_c}_{Clouds\ \ Albedo} \tag{4.11}$$

There Abs_{Atm} refers to the SW flux absorbed by the atmosphere (namely water vapour and CO_2 which are the only components whose concentrations vary with time). Such a decomposition allows to separate the feedbacks since any change in a physical quantity will only modify its own contribution. Note that along the run, $SW_{s\downarrow}$ was constant. Each term of equation 4.11 is integrated on Earth to provide a global value of $\Delta SW_{t\uparrow}$.

To evaluate Abs_{Atm}, we use the assumption that the SW flux is absorbed either by the atmosphere or by the Earth. In fact the contribution of clouds to the absorption is weak. It is easy to evaluate the flux absorbed by the Earth by the SW budget and the global flux absorbed from the TOA SW budget. We deduce the value of Abs_{Atm} as:

$$Abs_{Atm} = \underbrace{(SW_{t\downarrow} - SW_{t\uparrow})}_{Total\ \ Absorption} - \underbrace{(SW_{s\downarrow} - SW_{s\uparrow})}_{Earth\ \ Absorption} \tag{4.12}$$

from which ΔAbs_{Atm} can be directly inferred.

To evaluate the variation of surface albedo (in cloudy conditions) we use definition 4.2. The values of $SW_{s\downarrow}$ (195W.m^{-2})and α (0.14)are taken from control runs. Eventually we evaluate the variations of clouds albedo effect by calculating those of $SW_{t\uparrow} - SW_{s\uparrow}$. The crucial point of the method is the energy conservation. In fact, in equation 4.11 we calculate separately the left-hand term (9W.m^{-2}) and the right-hand terms (that summed give 9.3W.m^{-2}. It highlights that our flux decomposition did not forget any major term, which gives sense to assumptions 1 and 2. Moreover, it gives a quantitative idea of the coupling of the feedbacks, which were assumed to be of second-order.

4.4.2 Longwave

The LW analysis is harder since all mechanisms modify the greenhouse effect but only one measure of the total greenhouse effect can be defined, in CS and total-sky conditions. We define the greenhouse effect (GE) as:

$$GE = LW_{s\uparrow} - LW_{t\uparrow} \tag{4.13}$$

Hence we have:

$$\Delta LW_{t\uparrow} = \Delta(LW_{s\uparrow} - \Delta GE) \tag{4.14}$$

where $LW_{s\uparrow}$ is an output of the model and corresponds to the unique black-body radiation of Earth.

We can also define the clouds radiative forcing CRF as:

$$CRF = GE_{cs} - GE_{tot} \tag{4.15}$$

where *tot* refers to total sky.

The CRF contains the direct effect of clouds and the indirect effects, namely overlap with other LW absorbers.

We now have to explicit GE:

$$GE = GE_P + GE_{LR} + GE_{CO_2} + GE_{vap} + GE_{cl} \tag{4.16}$$

The Planck greenhouse effect comes from the non-linearity of Stefan's law as already discussed. It is defined as the difference between the surface radiation increase and the Planck feedback:

$$GE_P = (4\sigma\Delta T_s^3 - \lambda_P)\Delta T_s \tag{4.17}$$

It is calculated for a vertically uniform change in temperature. Nonetheless, climate simulations also enhance changes in lapse-rate. A simple model (see annex C) gives an evaluation of this effect. In this very model, a change in lapse rate modifies the emission of LW radiation towards space by the amount:

$$\Delta N_{LR} = 4\sigma T_t^3(\Delta T_t - \Delta T_s)(1 - \beta) \tag{4.18}$$

where T_t is the temperature at the tropopause, and T_s the surface temperature. We consider the lapse rate to be vertically uniform, as well as the lapse rate variation and ΔT_t and ΔT_s refer to the tropopause and surface temperature changes observed. β depends on the atmosphere optical thickness. The expression is given for an atmospheric column and must be integrated on the whole surface of Earth to provide the value of the feedback.

Here comes the hardest point. We still still to evaluate the effects of water vapour, CO_2 and clouds. This is impossible from the simple evaluation of total-sky flux. That's why we deal with the greenhouse effect in CS conditions that can be computed from the simulation outputs:

$$\Delta GE_{cs} = \Delta GE_{P,cs} + \Delta GE_{LR,cs} + \Delta GE_{CO_2,cs} + \Delta GE_{vap,cs} \tag{4.19}$$

The first two terms of the right-hand side of Eq. 4.19 can be evaluated from the simple model of greenhouse effect, taking an appropriate clear-sky value for the

absorption of the atmosphere. It is clear that in CS conditions, the atmosphere is more transparent and hence the effect of Planck greater. From Soden et al. [2008] we get $\lambda_P, cs = 3.6$. We assume here that clouds have an emissivity of 1 and the global emissivity is calculated from a reference cloud cover of 70%. Hence the total sky emissivity is chosen equal to 0.9.

We also know the value of $\Delta GE_{CO_2,cs}$ from the regression method used in chapter 3. This provides the value of $\Delta GE_{vap,cs}$.

Now we can evaluate ΔGE_{vap} and ΔGE_{CO_2} given Assumption 3 (Table 4.4 summarizes the important values). $\Delta GE_{CO_2,cs}$ has to be multiplied by 0.75 and $\Delta GE_{vap,cs}$ by 0.68. The only remaining term in 4.16 is thus the clouds greenhouse effect.

Gas	Individual contribution	Combined with overlap effects
H_2O	71 (49)	75 (51)
CO_2	29 (22)	32 (24)
Overlap H_2O–CO_2	7 (4)	
O_3	8 (7)	10 (7)
Overlap with O_3	2	
$CH_4 + N_2O$ + ovlp	8 (4)	8 (4)
Total	**125 (86)**	**125 (86)**

Gas	Clear sky	Cloudy sky
H_2O	43	38
CO_2	1	0
O_3	14	15
O_2	2	2
Overlap effects	0	12
Total	**60**	**67**

Figure 4.4: Clear and cloudy sky LW (up) and SW (bottom) radiative forcings ($W.m^{-2}$) and the contribution of individual greenhouse gases to this total. Cloudy sky results are in parentheses (from Kiehl and Trenberth [1997])

Eventually we get the expression of each λ_i from the linear evolution of the flux along the ramp experiment and from the fast response analysis:

$$N_i = \Delta Q_{i,fr} - \lambda_i \Delta T_f \tag{4.20}$$

$$\lambda_i = \frac{1}{\Delta T_f} (\Delta Q_{i,fr} - N_i) \tag{4.21}$$

4.4.3 The step approach for the SW decomposition

We used the ramp experiment for the decomposition of the net TOA radiative budget. However, it is evident that the same analysis could have been done from the step experiment. We have done it for the SW budget following decomposition 4.11 and found almost exactly the same feedbacks. It is interesting to see that the feedback parameters seem insensitive to the forcing applied, which is a characteristic of a

linear system. Using this SW decomposition for the step experiment and the regression method (versus ΔT) provides straight forward the fast response of a particular process and its feedback parameter.

For the LW decomposition, we still face the same problem: it is impossible to get an evident decomposition of the greenhouse effect. We have from the clear-sky and total sky decompositions the following system of equations

$$\lambda_{LN} = \lambda_{P,cs} + \lambda_{vap,cs} + \lambda_{LR,cs} \tag{4.22}$$
$$\lambda_{LC} = (\lambda_P - \lambda_{P,cs}) + (\lambda_{vap} - \lambda_{vap,cs}) + (\lambda_{LR} - \lambda_{LR,cs}) + \lambda_{cl,LW} \tag{4.23}$$
$$\lambda_{vap,cs} = 1.45\lambda_{vap} \tag{4.24}$$
$$\lambda_{LR,cs} = 0.26\lambda_{LR,cs} \tag{4.25}$$

where the last two equalities are deduced from Kiehl and Trenberth [1997] and from our model of greenhouse effect, respectively. However, we have 5 unknowns but only 4 equations which means that more assumptions still have to be made to get a solvable system. Whatever the method used, we cannot get a simple decomposition of the LW response.

In a word, the step analysis provide easily the fast responses and gives a good evaluation of the feedback parameters (for the SW component), while the regressions are clearly linear. Nonetheless, we have to extrapolate the curves for very short periods which implies a part of subjective interpretation. On the contrary, for processes that might be less clearly linear with time, the ramp analysis provide a curve that can be approximated by a right, although it is not one at the beginning or at the end of the experiment. The ramp allows us to focus on the short time scales thanks to its selectivity.

4.5 Results

The ultimate goal of the method introduced is to evaluate a posteriori the contribution of each feedback to the net TOA flux. We summarize in table 4.5 the contributions to the net budget and the associated feedback parameters (calculated from 4.21) given that $\Delta T_f = 5K$).

We note that the total feedback parameter calculated this way (essentially from the ramp analysis) is quite close to the one found for the direct regression on the step experiment ($\lambda = 0.77$). Moreover, at the end of the ramp run, we have a net TOA budget $N = 2.8\text{W.m}^{-2}$ (see figure 2.6) which is coherent with $N - \Delta Q = -3.7\text{W.m}^{-2}$ since $\Delta Q = 6.5\text{W.m}^{-2}$. This highlights the idea that this method is based on energy conservation, the net budget calculated from the various contributions being the same as the net budget given by the model output.

We give in table 4.5 the feedbacks we obtained and compare it to the results of Dufresne and Bony [2008](we take the mean of all models presented) and to the former IPSL model (taken from Soden and Held [2006]). We also use the multimodel

	$N_i(W.m^{-2})$	$\Delta Q_{i,fr}$	$\lambda_i(W.m^{-2}.K^{-1})$
LW			
Planck	-16		3.2
Lapse Rate	-4.25		0.85
Water Vapour	5.5		-1.10
Clouds	3.37	-1.58	-0.99
CO_2		4.89	
Total LW	-9.8		1.96
SW			
Water Vapour	0.35		-0.07
Clouds albedo	6.5	2.14	-0.87
Surface albedo	1.8		-0.36
CO_2		0.84	
Total SW	6.5		-1.30
Total	**-3.3**		**0.66**

Table 4.1: Summary of the feedbacks we obtained with our flux decomposition

(IPCC AR4) ensemble-mean feedbacks provided by the GFDL Kernel method (Soden et al. [2008]), which separates SW and LW contributions of water vapour. We insist that the feedback parameter of the actual model is lower than any of the CMIP3 models. Our analysis provide a greater cloud feedback and a lower water vapour feedback than usually. It can be explained by the difficult distinction of both feedbacks in the LW in total sky, but we also point out that the very low total feedback found for the current IPSL model requires a singular change in the model behaviour compared to former studies. Our method distinguishes between LW and SW clouds feedback. Usually clouds feedback is retrieved from the residual part of λ_{tot} and hence no specific SW or LW contributions is attributed to the clouds. As a consequence, our qualitative comparison is limited by the number of existing references.

	λ_{new} (W.m^{-2}.K^{-1})	λ_{mean}	λ_{old}	λ_{Kernel}
Planck	3.2	3.2	3.24	3.25
Lapse Rate	0.85	0.84	0.84	0.95
Water Vapour	-1.17	-1.8	-1.83	-1.9
Albedo	-0.36	-0.26	-0.22	-0.3
Clouds	-1.86	-0.69	-1.06	-0.79
Total	0.66	1.27	0.98	1.21

Table 4.2: Comparison of the feedbacks we obtained to former studies

4.6 Radiative budget of the Earth after CO_2 quadrupling

Straight ahead from the previous sections we can explicit the radiative budget of Earth in global warming conditions, following Trenberth's representation. We have obtained the variations of N and attributed them to various mechanisms. Extrapolating the variations until equilibrium from the values inferred of λ_i we define the flux variation for a process i as:

$$\Delta N_{i,eq} = \Delta Q_{i,fr} + \Delta N_{i,f} \frac{\Delta T_{eq}}{\Delta T_f} \tag{4.26}$$

We presented on figure 4.2, in parenthesis, the approximate new radiative budget found from our flux analysis.

4.7 Conclusions

In this chapter, we developed a new method to determine specific climate feedbacks. It is based on energy conservation and is computationally very easy. It is based on the decomposition of TOA net flux along a perturbed climate experiment on various contributors. We highlighted that given some assumptions the decomposition in the SW is very efficient while it remains arbitrary in the LW since all phenomena interact altogether through greenhouse effect. However, our method provides quantitative feedbacks that can be compared to other methods. For the particular case of the IPSL model analysis we showed that the clouds feedback seem greater than usually while the water feedback seems lower. This statement has to be considered with the scope of a particularly high sensitivity of the actual IPSL model compared to former studies.

CHAPTER 5

APPLICATION TO THE POLAR AMPLIFICATION

When the topic of global warming is tackled, reference is often made to the melting of ice sheet at high latitudes and the sea surface elevation. The first phenomenon is observed in the Arctic region where the summer extension of sea ice has roughly diminished in the last decades (the most marked event occurred in 2007). The sea surface elevation is due to the dilatation of water with temperature increase but also to the melting of glaciers on continental ice, in Greenland and Antarctic (the latter can be of potentially very large amplitude). Global warming at high latitudes has become a critical issue and both observations and simulations exhibit a more intense warming at these latitudes than at mid-latitudes. Although the term "polar amplification" is always used to describe the relative intensity of the warming, we'll precise that this should rather be called "Arctic amplification" since the warming of Antarctic, effective mainly around coastal areas and in the Peninsula, is not that high within the continent.

5.1 Origins of the polar amplification

Many studies have discussed the origin of the intensification of the warming at high latitudes. The classic idea was to attribute the Arctic warming to its strong surface albedo feedback. Works of Budyko (Budyko [1969]), Hall (Hall [2004]) explained and quantified the role of sea ice on the Earth radiative budget and the consequences of a large scale sea ice shrinking. Once sea ice has vanished from the ocean surface, the latter can absorb more solar radiation which leads to a local warming. Moreover, the atmosphere now in contact with the ocean will warm up while previously ice was isolating air from water. Since the albedo effect is easy to understand, later studies have focussed on the relative importance of the albedo factor. Lu and Cai (Cai [2005],Lu

and Cai [2010]) and Alexeev (Langen and Alexeev [2007]) have analysed the role of dry sensible heat transport, fixing the albedo and prohibiting any water transport. They showed that a greenhouse forcing would tend to amplify the poleward heat transport and thus have more impact at high latitudes. This is paradoxical since an increased poleward transport should correspond to a stronger meridional temperature gradient. In fact, the greater warming occurs at the equatorial tropopause, because of the higher greenhouse effect of water vapour there. This amplified meridional gradient at high altitude allows sensible heat to be transported poleward, in spite of a diminished surface gradient (due to the polar amplification). Studies taking into account water transport highlight that the dynamical effect is amplified by latent heat and water transport. Indeed, more water vapour is transferred from lower to higher latitudes where it will increase the greenhouse effect. Essentially, polar amplification can be seen as an amplification of the usual poleward heat transport. In (Winton [2006]), the author performed experiments of global warming with and without surface albedo and pointed out the relatively weak effect of sea ice feedback in the polar warming process. We should precise that the simulations performed in the previous studies did not take into account the asymmetry between the northern and southern hemispheres since some of them used aquaplanet models. The processes presented are thus general dynamical responses to an external forcing but differences between Arctic and Antarctic will be the core of the forthcoming discussion.

In a word, we want to explain the asymmetry featured on figure 5.1 (bottom), representing the zonally averaged temperature change at the end of the 250 years run consecutive to the step forcing. On figure 5.1 we represent the surface warming at the end of the same experiment to highlight more local features. This map puts forward the singularities occuring around the Antarctic continent. In fact in this area the mixed layer is very deep and thus waters keep their initial temperature as a result of a strong mixing. The warming is concentrated on continents and is the strongest in the Arctic ocean. On the contrary it is rather weak in continental Antarctic and in Greenland, which underlines the strong difference between sea ice and continental ice sheets.

5.2 Seasonal variability of the amplification

Trying to associate polar warming to physical feedbacks, we plotted the temperature change along the year. Figure 5.2 shows, month after month, the value of ΔT. We use a seasonal average of years 2100 to 2110 of the step experiment (starting in 1850). The first striking point is the strong seasonal variability at high latitudes (North and South)of the warming. On the contrary, at lower latitudes, the warming seems uniform along the year. The second even more intriguing point is that the larger change in temperature in polar regions occurs in winter, while one might assume it would occur in summer, because of the strong surface albedo feedback. This variability is particularly marked in Arctic (see figure 5.2). We present a qualitative explanation of this apparent strong variability (this is discussed in Boé et al. [2009]). In summer,

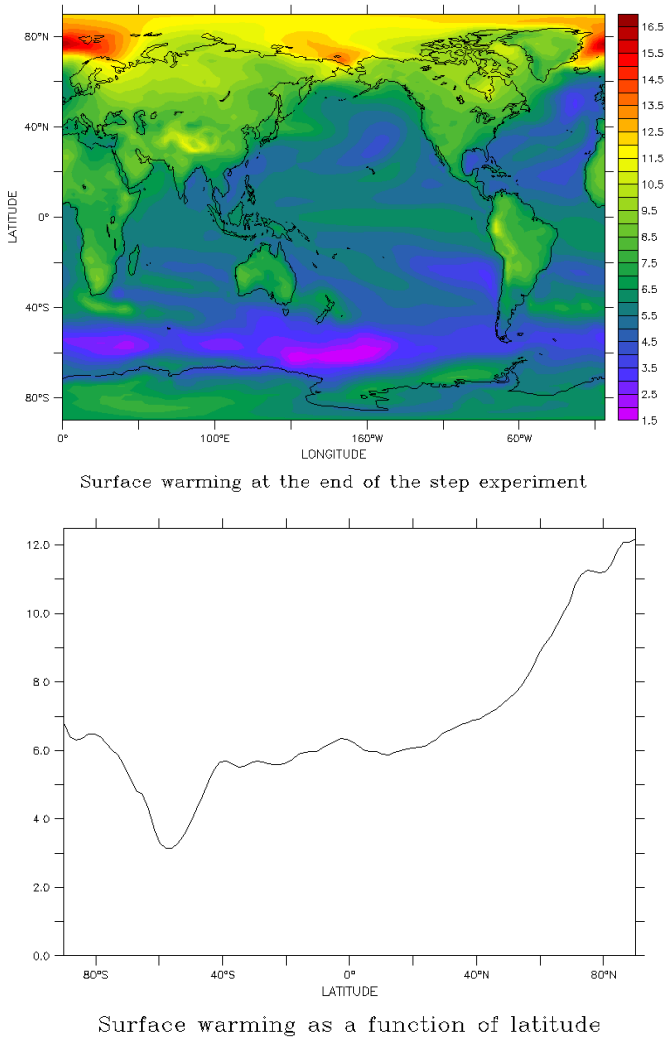

Figure 5.1: Average surface warming at the end of the step experiment

the atmosphere, though cold, has more or less the same temperature as the ocean. Thus, the isolation due to ice in summer is lesser than in winter. In addition, solar radiation is used to melt ice but cannot warm up the ocean significantly. On the contrary, in early winter, if ice has not totally reformed, then the atmosphere is not isolated from the ocean and the surface temperature has to be close to the ocean temperature, while it used to be much colder in presence of thick ice. This is why the warming is that marked in early winter. Nonetheless, one should keep in mind that dealing with the surface temperature can provide such surprising results, and changes at higher altitudes might have more sense. This interpretation is supported by the seasonal sea ice cover changes, which highlight that the larger relative vari-

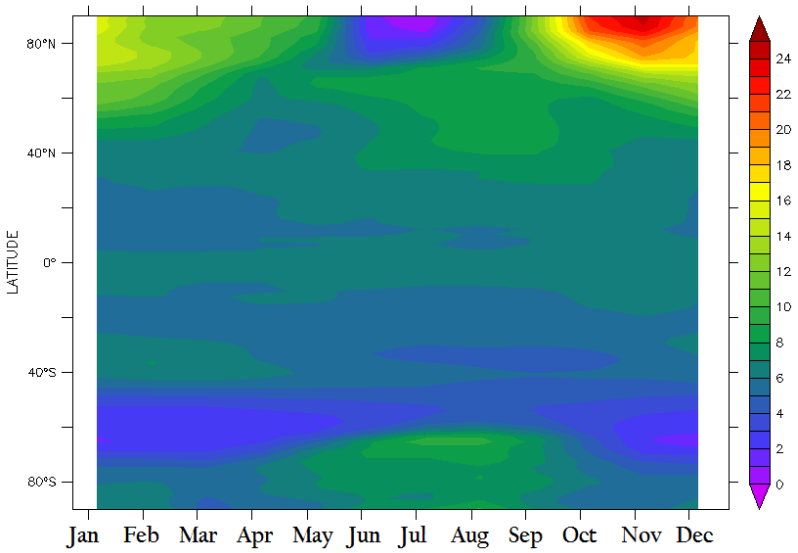

Figure 5.2: Seasonal variation of the surface temperature anomaly

ation occurs in early winter (see figure 5.3). Another qualitative interpretation is that CO_2 tends to uniformise seasons since greenhouse effect enhances the LW part of the Earth surface budget, in opposition to the solar contribution. Hence a greater warming in winter, when only the LW component can modify the net energy budget.

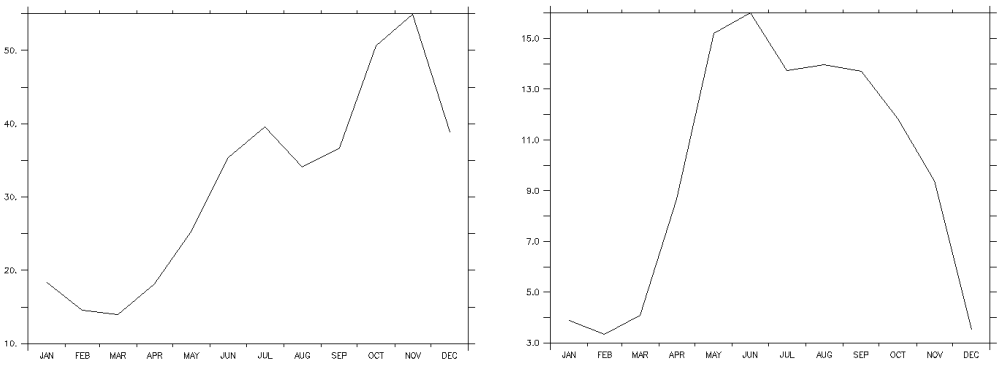

Figure 5.3: Seasonal relative variation of sea ice cover in Arctic (l.) and Antarctic (r.) at the end of the ramp run

Although we have provided an explanation to the seasonal variation of polar warming, a deeper analysis of the Antarctic case show that a similar (smaller) variability is observed within the continent. The sea ice interpretation is less efficient in the Southern hemisphere and further analysis should be led to analyse other phenomena implicated in this seasonal variability.

5.3 The singularity of Antarctica

5.3.1 An isolated continent

In this section, we try to explain why Antarctica does not experience the same warming as in Arctic. Indeed, aquaplanet simulations predict a dynamical polar warming but the reality of the Earth morphology leads to others features. We make a link here between the physical isolation of Antarctica and its delayed warming.

As we can see on figure 5.1 the least surface warming is located at $60°S$ in the area of the Antarctic circumpolar current (ACC). This is due to the strong heat capacity of the surface ocean there, where the mixed layer is about $2000m$ deep. The ACC is also a region of mainly zonal circulation, and might be a barrier to flux towards Antarctica. We now give more quantitative evidence that Antarctica is energetically isolated. Our goal is to show that contrarily to Arctic regions, the net heat flux (sensible and latent) from tropical to Antarctic regions are weak.

On figure 5.4 (right) we plot both the TOA (red) and surface (black) net flux differences along the ramp experiment as a function of latitude. At a given latitude, the difference between the two curves corresponds to an ingoing (outgoing) meridional flux towards (from) an atmospheric column. We see that most of the equator surplus is redistributed towards higher latitudes. This supports the fact that an increased greenhouse effect forcing corresponds to an amplification of the repartition of solar radiation plotted on figure 5.4 (left). This is why the CO_2 forcing will be linked to an increased poleward transport. Nonetheless this statement is not true for the Antarctic region, where the net surface flux variation is more or less equivalent to the TOA net flux variation, highlighting a globally energetic isolation of the Antarctic continent along the experiment. On the contrary this is not true in Arctic regions where the same argumentation points out a strong poleward heat flux there. We present on figure 5.5 a map of the difference between TOA and surface net flux variations. Are coloured only areas where the difference is comprised between -10 and 10W.m^{-2}. Clearly Antarctica appears as isolated as far as enhanced poleward heat transport is concerned.

5.3.2 A dry continent

Another particularity of the Antarctic region is its extreme drought. The water vapour content there is about 4 times lower than in Arctic (2 vs 8 kg.m^{-2}) and precipitations about 3 times lower (10 vs 30 cm.yr^{-1}). As polar warming is partially explained by a poleward transport of water vapour, we see that this phenomenon is smaller in the southern hemisphere. However, water vapour has to be considered from two points of view. While the net latent heat transport towards Antarctic is weak, water vapour also has a strong warming effect as a greenhouse gas. The latter effect will be discussed later. The isolation of Antarctic might give an explanation to the weak warming predicted by experiments, since the water vapour feedback and the dynamical processes have been shown to be blocked by the strong zonal circulation

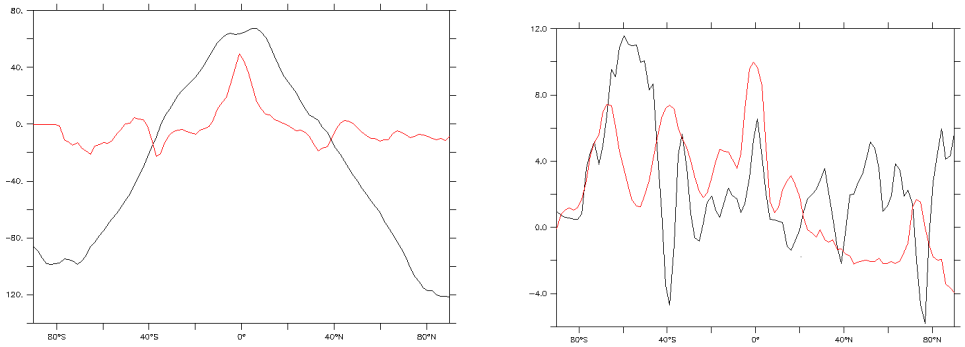

Figure 5.4: The climatological repartition of energy at TOA (black) and surface (red) with latitude (l.) and the variations of TOA (red) and surface (black) net radiative budget at the end of the ramp experiment (r.)

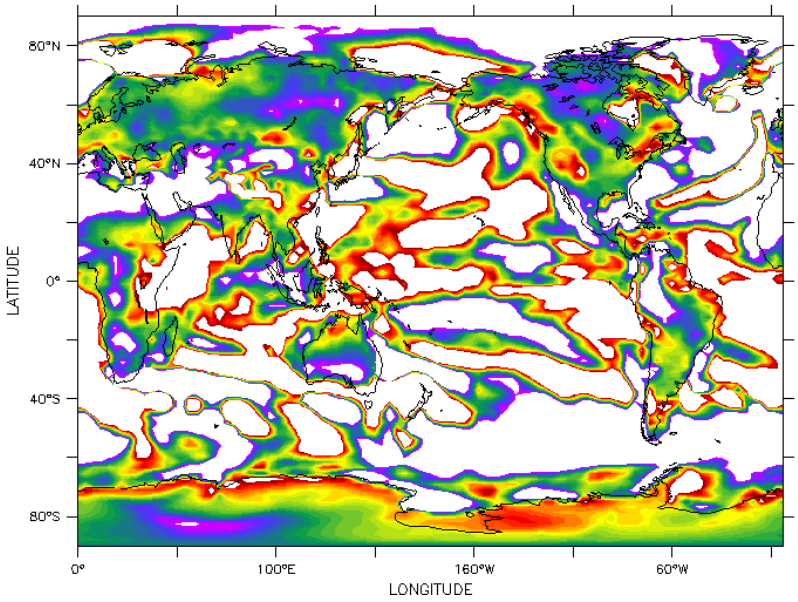

Figure 5.5: Variation of the difference between TOA and surface net flux

of the ACC.

5.4 Asymmetry of the amplification

Now that we have given a straight interpretation of the Antarctic particularity as far as polar warming is concerned, we will dwell on more quantitative comparisons, analysing with more accuracy the effects of each feedback and the response times of the various regions. We define the polar amplification (PA, for both poles) as the

ratio of the polar temperature change ΔT_p to the global temperature change ΔT_g (where we did not take into account the contribution of the Arctic region). This reads:

$$PA = \frac{\Delta T_p}{\Delta T_g} \tag{5.1}$$

where the polar regions correspond to the latitudes $[90°S, 70°S]$ and $[70°N, 90°N]$.

On figure 5.6, we present the evolution of the PA for both polar regions for the step experiment. The striking point is the difference in the shape of the two curves (on the left). In Arctic, PA is first increasing for a few decades before diminishing approximately linearly with time to an end-of-run value of about 2. On the contrary the Antarctic polar amplification constantly increases with time, with a change of slope after a few decades, as well. We interpret this feature in terms of characteristic times. Arctic tends to have a quick response to the step forcing (relatively to global Earth) and thus warms up quickly but much less after a few decades (this can be seen on the right panel of figure 5.6, where the initial slope of the Arctic warming is clearly steeper than for the average global warming). On the contrary, Antarctic seems to have a longer response time since its PA goes on increasing, illustrating a stronger warming relatively to the global Earth. The results of the exponential analysis are presented in Table 5.1. Given that Arctic is not horizontally isolated at all, these values have to be considered cautiously. The qualitative result fits perfectly with the earlier analysis of the temperature curves in terms of longer and shorter exponential terms. Moreover, the apparent linearity of the signals on each period can easily be explained by calculations from the linear electrical circuit. The question now is to provide a physical interpretation to the difference in the response time of the opposed regions. We explain further why Arctic seems to be more dependent on short time scales (concerning atmospheric and continental feedbacks) while Antarctic seems definitely governed by the long term deep ocean response.

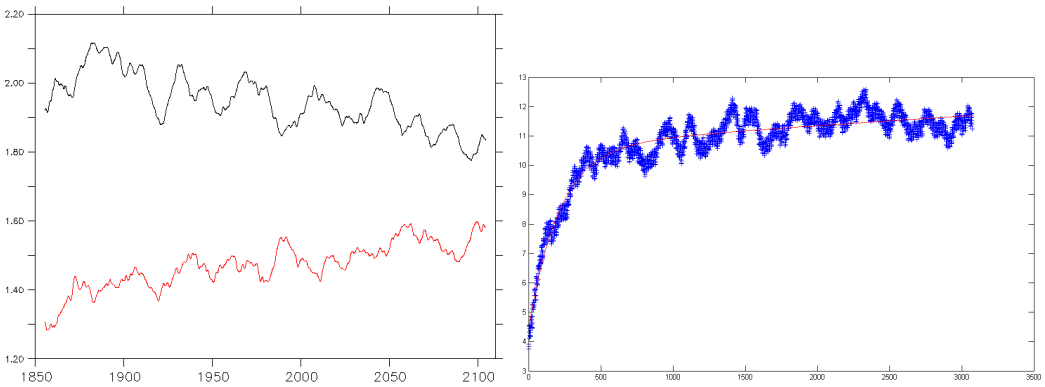

Figure 5.6: Evolution of the PA for the step experiment for Southern (red, 0.6 were added) and Northern (black) poles (l.). Evolution of the Arctic average surface temperature along the step experiment (r.)

	ΔT_{eq}	A	B	τ_1	τ_2
NP	15.2	6	5	18	950
SP	8	2.3	4	15	320

Table 5.1: Characteristics of Arctic and Antarctica average temperatures for the step experiment, following the electrical formalism

5.5 The feedbacks in polar regions

5.5.1 Application of the feedback analysis to polar regions

The method presented in chapter 4 is now applied to the polar regions. The method lies on the simple energy budget given by equation 1.1, which seems true for the whole Earth. We plotted the same regression for both polar regions and concluded that this simple equation has sense in Antarctic, but not at all in Arctic. Nevertheless, we provide in table 5.2 the feedback analysis obtained for Antarctica and extended it to Arctic to compare the results, although the latter results must be handled with care. The cloud feedback is illustrated on figure 5.8.

	Arctic	Antarctica	Total
LW			
Planck	3.2	3.2	3.2
Lapse Rate	-0.08	0.16	0.85
Water Vapour	-0.63	-0.76	-1.10
Clouds	-0.75	-0.71	-0.99
Total LW	1.74	1.91	1.96
SW			
Water Vapour	-0.22	-0.73	-0.07
Clouds albedo	0.73	0.56	-0.87
Surface albedo	-1.67	-0.47	-0.36
Total SW	-1.16	-0.64	-1.3
Total	**0.58**	**1.27**	**0.66**

Table 5.2: Feedback analysis applied to Arctic and Antarctica

There are many points to highlight in table 5.2. First of all, we see that the albedo feedback is greater at high latitudes than averaged on Earth, which was predictable. The lapse rate feedback is very low for both polar regions and the sign is even different for both. This feedback is illustrated on figure C.2. More generally, the sensitivity of the Northern Pole is greater than anywhere else, while the Southern Pole is all in all not very sensitive to the external forcing, which tends to polarize the so-called polar amplification rather towards Arctic. Eventually we underline that the water vapour feedback is greater for Antarctic which is coherent with the

previous analysis of Antarctic relative drought (see figure 5.7). Since the atmosphere is far from absorption saturation, any increase in a dry atmosphere will have more consequences than in an already humid one.

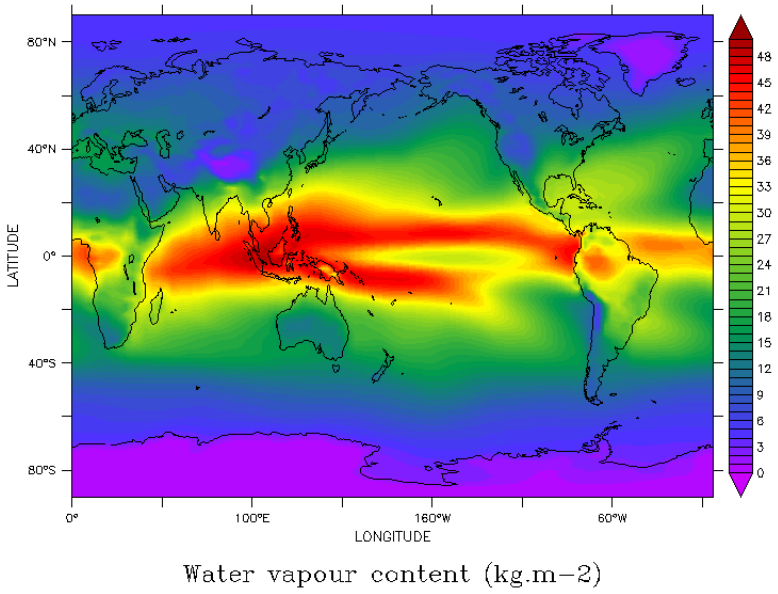

Figure 5.7: Climatological water content (in kg.m^{-2})in the atmosphere

5.5.2 The question of albedo

Antarctic and Arctic regions are fundamentally different as far as their albedo feedback is concerned. Indeed, Arctic is essentially an ocean seasonally covered by sea ice. This layer of ice both acts as a reflective surface and a physical isolator between the atmosphere and the ocean. In a warming scenario, melting of ice leads to a strongly diminished albedo since the formerly ice-covered surfaces ($\alpha \simeq 0.8$) become ice-free areas characterized by ocean albedo ($\alpha \simeq 0.15$). As a matter of fact the Earth global albedo might be diminished as well and the net flux TOA changed. The Earth, and more especially the Arctic region, would absorb more solar radiation and warm up. This is clear that the surface albedo feedback is positive since warming decreases the albedo which in return leads to an even greater warming.

On the contrary Antarctica is an ice-covered continent (whose area is about $14 \times 10^6 \text{km}^2$). Although there is sea ice all over the continent the proportion of the Antarctic area covered by sea ice threatened by imminent melting is significantly smaller than in Arctic. Let consider a warming in Antarctica, melting the continental ice would not change quantitatively the ice albedo since there will always remain ice underneath (at least on short time scales). In fact the crucial questions in Antarctica concern more the run-off from the glaciers to the Southern ocean which might lead to

an important sea elevation. Moreover, the evaluation of albedo variations in Antarctica must take into account the metamorphism of snow with ageing, the microscopic shape of snow and maybe the thermodynamic transformations that modify the ice structure. In the IPSL model, we noticed that the albedo on the continent does not change along a 250-year-long run which indicates that such physical models are not yet included in this GCM. In Antarctica essentially coastal sea ice can provoke albedo changes.

5.5.3 The clouds feedback

To illustrate the clouds feedback in polar regions we plotted the evolution of clouds at any latitude along the ramp experiment. Figure 5.8 features the results. Contrary to the average clouds evolution, clouds albedo has a negative feedback in polar regions. In fact, we see that low altitude clouds tend to increase with time in Arctic. This is not as simple in Antarctic. Indeed, we see that low altitude clouds tend to decrease while high altitude clouds tend to increase. We give two interpretations of this paradoxical result. First, we can imagine that the assumptions made for our flux decomposition are not valid in polar regions, especially the assumption that there is no atmosphere absorption after ground reflection. Second, the high altitude clouds might have a real impact on the planetary albedo if they are not as thin as assumed. In these polar regions, the greenhouse effect of clouds is enhanced in warming conditions, and for the Arctic region, the clouds responsible for this greenhouse effect seem to be medium level clouds while in Antarctica they might be higher clouds.

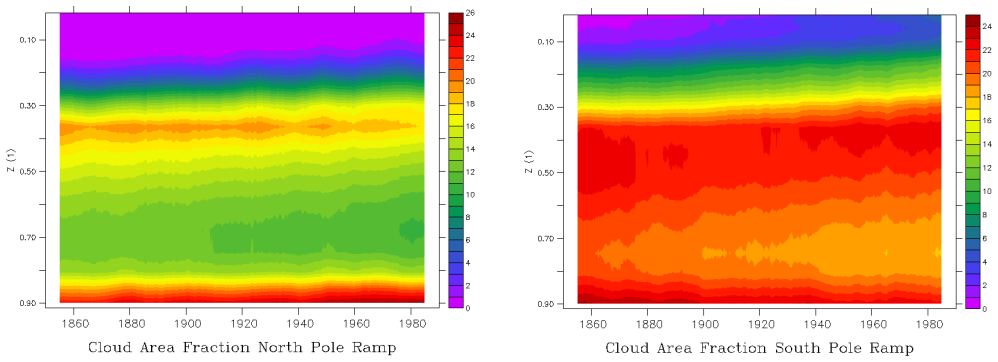

Figure 5.8: Evolution of the clouds in Arctic (l.) and Antarctica (r.) at any level of the model

5.6 Conclusions

We applied the method developed in chapter 4 to polar regions defined as $[90S, 70S]$ and $[70N, 90N]$. We highlighted that this method based on energy conservation was acceptable in Antarctica but not in Arctic. However we applied it to Arctic to

have enable comparisons between polar regions. We explained that the relatively low Antarctic albedo feedback came from the prescription of a constant albedo ($\alpha = 0.77$) in the inner continent. We also pointed out that despite the very low water content of the Antarctic any small increase could have important consequences for the greenhouse effect. We found that Arctic was very sensitive ($\lambda = 1.27$) to climate change while Antarctica seems less sensitive ($\lambda = 0.58$), which is probably due to its physical isolation.

CONCLUSION

Along this report we have insisted on the apparent linearity of GCMs simulations. We proposed a frame to interpret this linearity, introducing a simple climate energy budget. It reproduced well the real outputs of the IPSL model sot that it gave some weight to our physically based simple model. Although classically the physical objects that are discussed in papers are the sensitivity (or λ)and the equilibrium temperature change, we propose a simple method to evaluate the transient temperature change from either the step or the ramp experiment. This transient temperature is in fact the faster climate response, the temperature change that occurs rapidly after a forcing is imposed. The knowledge of this committed temperature can give a short-term prediction of the global warming. Our method is simple and does not require the model to reach equilibrium to get such interesting values. Moreover any kind of forcing can be applied to the electrical circuit without any computational requirements.

In a second part we introduced a diagnostic and inclusive way of evaluating climate feedbacks from a perturbed climate experiment. The method is very simple and efficient for the SW feedbacks. However, the LW analysis is harder and the feedbacks of lapse rate, clouds and water vapour entangled so that it has not much physical sense trying to separate them. The comparison with former studies is not much significant since the total sensitivity of the actual IPSL model is too different from the one evaluated with former methods. The same analysis was applied to polar regions, even though the theoretical frame of application was not verified in Arctic. It highlighted the strong sensitivity of Arctic while Antarctica had a sensitivity similar to the average one, but a much longer response time due to the presence of the ACC all around.

To conclude, we insist that our model fails in reproducing any non-linear features. In fact, some studies (eg.Gregory et al. [2004]) showed that λ might vary with time. It could be due either to the variation of a particular feedback (eg. when there is no ice anymore on Earth) or to a deep ocean feedback as was assumed in Winton et al.

[2010]. However, the electrical circuit could be improved by representing the inertia of the atmosphere but a study at shorter time scales would be necessary, which was not the goal of the present work. Climate feedback analysis is an attempt to quantify complex physical processes and thus can only be a very restrictive description of the climate evolution. It is currently a mean to compare the several existing GCMs but the way processes are isolated from each others in such an entangled system shows that it is hard a task.

Acknowledgements I am grateful to my supervisors Jean-Louis Dufresne and Alain Lahellec for rich, long and often late constructive discussions

APPENDIX A

A PHYSICAL INTERPRETATION OF κ

Usually, the so-called ocean heat efficiency κ is rather a result provided by models than the expression of a physical analysis. Up to now it has been used in the literature as a statement with no attempt to give it a physical interpretation (although it has been qualitatively tackled in Raper et al. [2002]). In this section we try to put some physics on this coefficient, by connecting it both to some vertical diffusivity and to the overturning circulation.

κ and the vertical diffusivity

In this paragraph, we discuss the physical meaning of κ in the relation 2.6. κ is a kind of diffusivity that quantifies the transfer of energy from the surface to the deep ocean through the mixed layer. We aim at quantifying the value of this flux-gradient heat efficiency. We use the same approach as MAGGIC introduced in Raper et al. [2001]. MAGGIC summarizes all the physics and results of GCMs in very simple box models. The goal is to obtain the equivalent of a huge GCM with only a few variables considered constant on the whole surface of Earth. For instance, in Solomon et al. [2007] (Table $S8.1$) one can find the values of the average forcing, the vertical diffusivity of the ocean and the effective climate sensitivity obtained from the MAGGIC models derived from GCMs used in IPCC (AR4). We use the values of the vertical diffusivity k_{dif} provided by this Table. From Dufresne and Bony [2008] we get the values of κ for the same corresponding GCMs. Trying to link κ to physical processes, we assume that it has a link with k_{dif}, that is why we analyse the correlation between those two and find that they are quite well correlated ($r^2 = 0.6$ for 11 models). We find that:

$$\kappa = 0.31\ k_{dif} + 0.2 \tag{A.1}$$

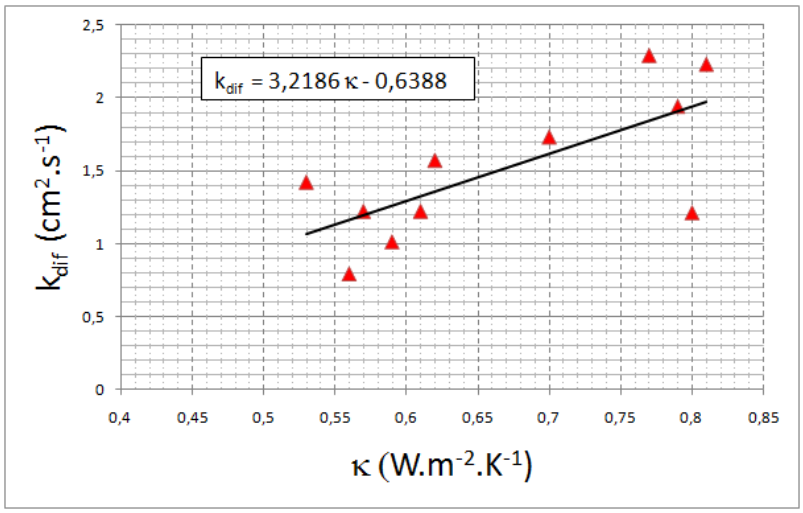

Figure A.1: Correlation of k_{dif} vs κ

We conclude that part of the heat transferred to the ocean corresponds to the diffusive mixing between the surface layer and the deep ocean. Nonetheless, the remaining term in Eq. A.1 should be accounted for by some other mechanism of heat transfer. The first idea is to look for some correlation between the strength of the thermohaline circulation predicted by the models and the corresponding value of κ. In practice, the thermohaline circulation is usually counted as the meridional overturning circulation in the Northern Atlantic. There are only few accurate measures available in the Atlantic and they are –maybe abusively– considered to be a measure of the global overturning circulation. For several GCMs, we got these values of this overturning circulation from Medhaug and Furevik [2011] and found that there is absolutely no correlation between the AMOC value and κ. That is why we develop our own simplistic model of the thermohaline circulation to explain the remaining term in A.1. From Eq. A.1 we deduce that even with no diffusivity, there would be a heat transfer from the surface into the ocean, that is why we focus on an advective transfer of energy.

A simple model of the overturning circulation

Our goal is to express κ as a sum of a diffusive and an advective term. The existence of a thermocline –a strong vertical gradient in temperature underneath the mixed layer– breeds a strong heat diffusivity from the hot surface to the colder deep ocean. At equilibrium, this downward heat flux should be balanced by a heat transfer from the deeper ocean to the surface. The latter contribution is a consequence of the

overturning circulation. We will now link the advective heat transfer due to the overturning circulation to the surface temperature change. Physically, we consider that a surface warming tends to diminish the overturning circulation (this topic is a critical one and is much debated). Thus, with an increase in surface temperature, the overturning circulation weakens. The net result of such a weakening is a net heat transfer towards the deep ocean (the latter heat release being diminished). To illustrate this, we use a 3-boxes ocean model and bound the linearly the intensity of the overturning circulation to the change in temperature by the expression provided in Raper et al. [2001]:

$$w = w_0 \left(1 - \frac{\Delta T}{\Delta T_M}\right) \tag{A.2}$$

where w and w_0 are the current and reference upwelling rates (in $m.yr^{-1}$) and ΔT_M a change in temperature that would stop the overturning circulation.

The model we use is based on the observed fact that in the overturning circulation, upwelling occurs almost everywhere in the oceans whereas deep water formation is concentrated in tiny areas around Greenland and Antarctic. The second assumption is that in conditions of global warming, before the deep ocean really responds, the temperature of the sinking and deep waters remain constant (see Raper et al. [2001], Fig.5). This is simulated by the models and comes from the very large heat capacity of the surface layer in deep water formation areas. In fact we retrieve κ considering ΔT_d is constant but extend the reasoning to get the expression 2.7 when the deep ocean has started to warm up.

We represent our model on figure A.2. large arrows represent the sense of the circulation and thinner ones represent diffusive heat transfer. From this scheme, we can deduce the energy budget of the deep ocean. Let's write the net advective heat flux into the ocean (per surface unit, where ρ and C_p are the water density and heat capacity):

$$N_{adv} = \rho C_p w_0 \left(1 - \frac{\Delta T}{\Delta T_M}\right)(T_p - T_d) \tag{A.3}$$

Thus, the change in net advective flux into the deep ocean due to the temperature change ΔT can be expressed:

$$\Delta N_{adv} = \rho C_p w_0 \frac{\Delta T}{\Delta T_M}(T_d - T_p) \tag{A.4}$$

We now give the expression of the diffusive flux that enters the deep ocean from the surface (note that we neglect the diffusive flux from the deep water formation areas to the deep ocean):

$$N_{dif} = k_{dif} \rho C_p \frac{T_s + \Delta T - T_d}{h_{th}} \tag{A.5}$$

where h_{th} is the thermocline depth.

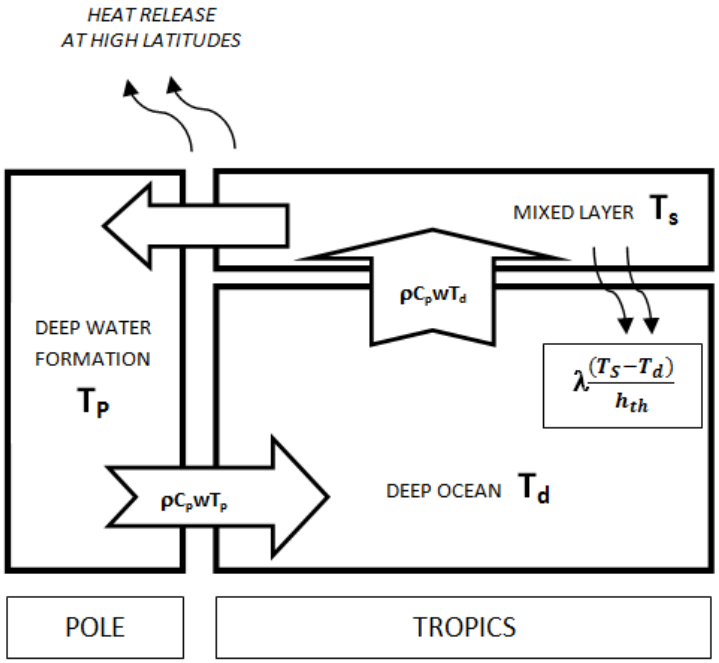

Figure A.2: 3-boxes model of the thermohaline circulation

In the same way, we can express the change in the diffusive flux due to the change in surface temperature:

$$\Delta N_{dif} = k_{dif} \rho C_p \frac{\Delta T}{h_{th}} \tag{A.6}$$

The next assumption is a critical one, since we consider that for no temperature change, the net advective flux upward balances the downward diffusivity. At equilibrium we assume that:

$$k_{dif} \rho C_p \frac{T_{s,eq} - T_d}{h_{th}} = \rho C_p w_0 (T_d - T_p) \tag{A.7}$$

so that the net flux into the ocean is given at any time by the sum $\Delta N_{adv} + \Delta N_{dif}$.

We have eventually the physical expression of $N \equiv \Delta N$:

$$N = \rho C_p \left(\frac{k_{dif}}{h_{th}} + w_0 \frac{T_d - T_p}{\Delta T_M} \right) \Delta T \tag{A.8}$$

We take $h_{th} = 1000m$ (see Raper et al. [2001], Fig.6), $w_0 = 4\text{m.yr}^{-1}$ (from Raper et al. [2001]), $\Delta T_M = 7\text{K}$, $\rho C_p = 4.2\ 10^6\ \text{J.K}^{-1}\text{.m}^{-3}$ and $T_d - T_p = 2\text{K}$. These values are consistent with equation A.7 given that $T_{s,eq} - Td \simeq 15\text{K}$. With these values,

and noticing that the ocean processes occur on only 70% of the Earth surface, we get

$$N = (0.3\ k_{dif} + 0.11)\Delta T \tag{A.9}$$

This latter equation, deduced from our simple model of the thermohaline circulation, fits well with the empirical correlation A.1. The diffusive process is rather well quantitatively explained. On the contrary, we find that the value of w_0 we used is not sufficient (it corresponds to an overturning circulation of 45Sv). Considering the problem differently, we now look for the value of w_0 that would explain the values of κ observed. We would need $w_0 = 7.3\text{m.yr}^{-1}$ which is equivalent to an overturning circulation of 85Sv. Comparatively, the strength of the AMOC is around 30Sv. This result implies that the global overturning circulation should be much greater than the Atlantic branch. Recently, the role of the Antarctic branch has been much discussed since there might be a very strong overturning circulation at these latitudes. For instance, [Garabato et al., 2007] suggests that the Antarctic overturning circulation might reach some 80Sv. Thus our results are not irrelevant and might be an indication that the heat transfer from deep ocean to atmosphere mainly occurs in Antarctic regions where the vertical upwelling is the stronger.

Remark In our physical interpretation of κ we proved that it is a global parameter, depending on the whole oceanic circulation, and not only on local conditions. As a consequence the equation 2.6 has a sense only for global energy budget. We plotted N vs ΔT for large polar regions (averages between 40° and 90°, where deep water formation is prominent). For these areas, there is absolutely no correlation between N and ΔT. This supports the introduction of a term associated to the overturning circulation.

APPENDIX B

APPROXIMATIVE DERIVATION OF THE ΔT SOLUTION FOR THE RAMP EXPERIMENT

We start from equation 2.14 from which we calculate

$$\frac{1}{t_f}\int_0^t \Delta T_{step} = \frac{1}{t_f}\int_0^{t'} \left(A\left(1 - e^{-\frac{t'}{\tau_1}}\right) + B\left(1 - e^{-\frac{t'}{\tau_2}}\right)\right) \tag{B.1}$$

$$= \frac{1}{t_f}\left[(A+B)t' + A\tau_1 e^{-\frac{t'}{\tau_1}} + B\tau_2 e^{-\frac{t'}{\tau_2}} \right]_0^t \tag{B.2}$$

We remember here that for this calculation we assume

$$\tau_1 \ll t' \ll \tau_2 \tag{B.3}$$

so that we can rewrite

$$\Delta T_{ramp}(t) = \frac{1}{t_f}\left((A+B)t + A\tau_1(e^{-\frac{t}{\tau_1}} - 1) + B\tau_2(e^{-\frac{t}{\tau_2}} - 1)\right) \tag{B.4}$$

$$= \frac{1}{t_f}\left((A+B)t - A\tau_1 + B\tau_2(1 - \frac{t}{\tau_2} - 1)\right) \tag{B.5}$$

The latter equation leads to the important result:

$$\Delta T_{ramp}(t) = \frac{1}{t_f} A(t - \tau_1) \tag{B.6}$$

This latter equation means that the value of $\frac{A\tau_1}{t_f}$ can be inferred from the linear regression of $\Delta T_{ramp}(t)$. We checked that the y-intercept of this regression was coherent with the values of A and τ_1 calculated previously.

From the equation 1.1 and given B.6 in conditions so that B.3 is true, we can give an approximation of N for the ramp experiment.

$$N = \lambda \left(\Delta T_{eq} \frac{t}{t_f} - \Delta T \right) \tag{B.7}$$

$$= \frac{\lambda}{t_f} \left((\Delta T_{eq} - A)\, t + A\tau_1 \right) \tag{B.8}$$

$$= \frac{\lambda}{t_f} \left(B \left(\frac{t_f \Delta T}{A} + \tau_1 \right) + A\tau_1 \right) \tag{B.9}$$

$$= \frac{\lambda B}{A} \Delta T + \frac{\tau_1}{t_f} \lambda \Delta T_{eq} \tag{B.10}$$

Given 2.30 this is exactly of the form

$$N = \kappa \Delta T(t) + C \tag{B.11}$$

This illustrates the linear regression of 2.6 and particularly the empirically positive y-intercept.

APPENDIX C

A SIMPLE MODEL OF GREENHOUSE THE GREENHOUSE EFFECT

Here we present a simple model of the atmosphere to illustrate the Planck, greenhouse and lapse rate effect. We assume that the absorption coefficient k_a is vertically uniform and the atmosphere is taken as a grey body. We start from the Stefen law that reads:

$$B(z) = \epsilon \sigma T(z)^4 \tag{C.1}$$

where $\epsilon = 1$ for the surface and $\epsilon = 0.9$ for a total-sky atmosphere. This was calculated from Kiehl and Trenberth [1997] using the TOA outgoing LW flux that comes directly from the surface (namely 40W.m^{-2}). The model has less sense for a clear-sky atmosphere since it can not really be treated as a grey body. Nonetheless we will take $\epsilon = 0.5$ for reasons explained further.

For more simplicity we linearise this equation, assuming that for any layer of the atmosphere, the grey-body law can be expressed as:

$$B(z) = B_0 + (z - z_0)\frac{B_t - B_0}{z_t - z_0} \tag{C.2}$$

where the subscript t and 0 respectively refers to *TOA* and *surface*

The figure C.1 represents the model used.

Let's now explicit the radiation absorbed by the layer $z + \Delta z$ that came from z:

$$I_z(z + \Delta z) = B(z) \exp\left(\frac{-k_a \Delta z}{\mu}\right) \tag{C.3}$$

where $\mu = \cos\theta$ represents the inclination of the radiation considered.

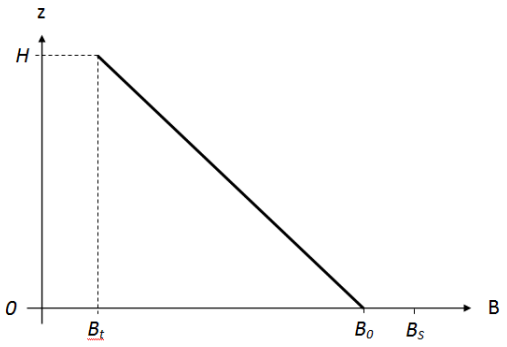

Figure C.1: Scheme corresponding to the simple model

We can now express the outgoing flux at TOA:

$$I_t = B_s \exp\left(\frac{-k_a H}{\mu}\right) + \int_0^t B(z) \exp\left(\frac{-k_a (H-z)}{\mu}\right) \frac{k_a}{\mu} \tag{C.4}$$

where H is the total height of the atmosphere

We can now An integration by parts reads:

$$I_t(x) = B_s e^{-x} + B_0(1-e^{-x}) + (B_t - B_0)\left[1 - \frac{1}{x}(1-e^{-x})\right] \tag{C.5}$$

where $x = \dfrac{k_a H}{\mu}$

At this point it is interesting to note that the emissivity of the atmosphere ϵ and its absorptivity k_a can be related by:

$$e^{-x} = 1 - \epsilon$$

which illustrates that $1-\epsilon$ is the part of the surface radiation that reaches TOA. This reads $x = 1.3$.

Let's now define the greenhouse effect (GE) as the difference between the flux radiated by the surface and the outgoing flux TOA :

$$GE = B_s - I_t = (B_s - B_0)(1-e^{-x}) + (B_0 - B_t)\left[1 - \frac{1}{x}(1-e^{-x})\right] \tag{C.6}$$

Eventually we rewrite it only in terms of the global emissivity:

$$GE = (B_s - B_0)\epsilon + (B_0 - B_t)\left[1 + \frac{\epsilon}{\ln(1-\epsilon)}\right] \tag{C.7}$$

We focus now on the impact of a change in temperature on the greenhouse effect. We will differentiate the Planck effect (only due to the change in equivalent temperature) from the lapse-rate effect due to the vertical non-uniformity of the warming. We consider first that the emissivity is unchanged in order to isolate the effect of temperature alone

This reads:

$$\Delta GE = \epsilon\Delta(B_s - B_0) + \left[1 + \frac{\epsilon}{\ln(1-\epsilon)}\right]\Delta(B_0 - B_t) \tag{C.8}$$

$$= 4\sigma\epsilon(1-\epsilon)T_s^3\Delta T_s + 4\sigma\left[1 + \frac{\epsilon}{\ln(1-\epsilon)}\right]\epsilon\left(T_s^3\Delta T_s - T_t^3(\Delta T_s + \Delta_{LR})\right) \tag{C.9}$$

$$= -4\sigma\epsilon\left\{\underbrace{\Delta T_s\left[(\epsilon - 2 - \beta)\,T_s^3 + (1+\beta)\,T_t^3\right]}_{Planck} + \underbrace{\Delta_{LR}T_t^3\left[1+\beta\right]}_{LapseRate}\right\} \tag{C.10}$$

where $\beta = \dfrac{\epsilon}{\ln(1-\epsilon)}$ and $\Delta_{LR} = \Delta T_t - \Delta T_s$

In the last equation, on the right-hand side, the first terms correspond to the GE due to a uniform increase of temperature, while the last term corresponds to the lapse-rate effect. We take for the numerical analysis, $T_t = 220K$ which is the tropopause average temperature and $T_s = 285,2$. The total-sky calculation led to $\lambda_p = 3,22$ which is relevant given classic values (see Soden et al. [2008]. Calculating Planck feedback parameter from formula C.10 and imposing that $\lambda_{P,cs} = 3,55$ provided the value of ϵ for clear-sky conditions. From this parametrization we assume the lapse rate GE is close to the second term of the right-hand side of equation C.10.

On figure C.2 we illustrate the way we determined Δ_{LR}. We use the change of temperature at the inversion level, where the warming starts decreasing (here about 300 hPa). The left plot gives a sense to the so called lapse rate feedback. Indeed, with the definition we chose of the lapse rate, we see that it is proportional to ΔT_s which is the definition of a feedback.

The effect of LW absorbers (water vapour and CO_2) can be determined following the same method and considering that the temperature profile is unchanged:

$$\Delta GE = (B_0 - B_s)\Delta\epsilon + (B_t - B_0)\Delta\left[1 + \frac{\epsilon}{\ln(1-\epsilon)}\right] \tag{C.11}$$

This decomposition allows us to associate to each physical process a change in the outgoing LW radiation, hence a contribution to the global change in temperature.

From this model we can also highlight the fact that a vertically homogeneous increase of the atmosphere temperature leads to a smaller increase in the radiative equivalent temperature. From C.5 we can introduce the notion of radiative equivalent temperature T_e as follows:

$$\sigma T_e^4 = \sigma\left\{T_0^4\left(e^{-x} + \epsilon(1-e^{-x}) - \epsilon\left[1 - \frac{1}{x}(1-e^{-x})\right]\right) + T_t^4\epsilon\left[1 - \frac{1}{x}(1-e^{-x})\right]\right\} \tag{C.12}$$

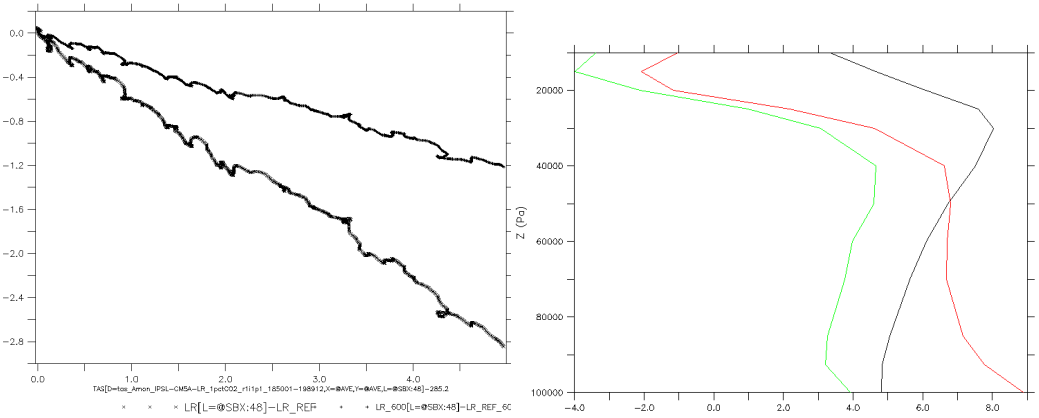

Figure C.2: (l.) The variation of the lapse rate as a function of ΔT_s along the step experiment for a reference at 600 (u.) and 300 (b.) hPa. (r.) Variations of temperature as a function of altitude at the end of the ramp experiment. Northern Pole is in red, southern pole is in green and global in black.

This leads to an expression of T_e^4 of the form:

$$T_e^4 = AT_0^4 + BT_t^4 \tag{C.13}$$

with $A + B = 1 - \epsilon + \epsilon^2 \leq 1$ and $A, B \geq 0$.

We can now express the variation ΔT_e:

$$\Delta T_e T_e^3 = \Delta T_0 \left(AT_0^3 + BT_t^3\right) \tag{C.14}$$

Multiplying both members of the latter equation by T_e and using C.13 we get:

$$\Delta T_e \left(AT_0^4 + BT_t^4\right) = \Delta T_0 \left(AT_0^3 + BT_t^3\right) \left(AT_0^4 + BT_t^4\right)^{1/4}$$

The function $x \longrightarrow x^{1/4}$ is concave, so that we obtain the inequality:

$$\Delta T_e \left(AT_0^4 + BT_t^4\right) \leq \Delta T_0 \left(AT_0^3 + BT_t^3\right) \left(\frac{A}{A+B} T_0 + \frac{B}{A+B} T_t\right) (A+B)^{1/4}$$
$$\Delta T_e \left(AT_0^4 + BT_t^4\right) \leq \Delta T_0 \left(AT_0^3 + BT_t^3\right) (T_0 + T_t)$$
$$\Delta T_e \left(AT_0^4 + BT_t^4\right) \leq \Delta T_0 \left(AT_0^4 + BT_t^4\right)$$

We obtain eventually the important relation:

$$\Delta T_e \leq \Delta T_0 \tag{C.15}$$

REFERENCES

T. Andrews, P. Forster, O. Boucher, and N. Bellouin. Precipitation, radiative forcing and global temperature change. *Geophysical Research Letters*, 37, 2010.

S. Arrhenius. On the influence of carbonic acid in the air upon the temperature of the ground. *Philosophical Magazine and Journal of Science*, 41:237–276, 1896.

J. Boé, A. Hall, and X. Qu. Current gcm's unrealistic negative feedback in the arctic. *Journal of Climate*, 22:4682–4695, 2009.

S. Bony, R. Colman, V. M. Kattsov, and R. P. Allan. How well do we understand and evaluate climate change feedback processes? *Journal of Climate*, 19, August 2006.

M.I. Budyko. The effect of solar radiation variations on the climate of the earth. *Tellus*, 21(5):601–613, 1969.

M. Cai. Dynamical amplification of polar warming. *Geophysical research Letters*, 32, November 2005.

J. C. Doran, P. T. Priscu, W. Berry Lyons, J. E. Walsh, A. G. Fountain, D. M. McKnight, and D. L. Moorhead. Antarctic climate cooling and terrestrial ecosystem response. *Nature*, January 2002.

J-L. Dufresne and S. Bony. An assessment of the primary sources of spread of global warming estimates from coupled atmosphere-ocean models. *Journal of Climate*, October 2008.

G. Forster, J. D. Annan, Schmidt G. A., and Mann M. E. Comment on "heat capacity, time constant, and sensitivity of earth's climate system" by s. e. schwartz. *Journal of Geophysical Research*, 113, 2008.

P. Forster and J.M. Gregory. The climate sensitivity and its components diagnosed from earth radiation budget data. *Journal of climate*, 2006.

P. Forster and K. E. Taylor. The climate sensitivity and its components diagnosed from earth radiation budget data. *Journal of Climate*, 19:39–52, 2006.

A.C.N. Garabato, D. P. Stevens, A. J. Watson, and W. Roether. Short-circuiting of the overturning circulation in the antarctic circumpolar current. *Nature*, 447, May 2007.

R. G. Graversen and M. Wang. Polar amplification in a coupled model with local albedo locked. *Climate Dynamics*, 33:629–643, 2009.

J. Gregory and M. Webb. Tropospheric adjustment induces a cloud component in co_2 forcing. *Journal of Climate*, 21:58–71, 2008.

J.M. Gregory and J.F.B. Mitchell. The climate response to co_2 of the hadley centre coupled aogcm with and without flux adjustment. *Geophysical Research Letters*, 24(15):1943–1946, August 1997.

J.M. Gregory, W. J. Ingram, M. A. Palmer, G. S. Jones, P. A. Stott, R. B. Thorpe, J. A. Lowe, T. C. Johns, and K. D. Williams. A new method for diagnosing radiative forcing and climate sensitivity. *Geophysical Research Letters*, 31, 2004.

A. Hall. The role of surface albedo feedback in climate. *Journal of climate*, 2004.

J. Hansen, A. Lacis, D. Rind, and G. Russell. Climate sensitivity: Analysis of feedback mechanisms. *Geophysical Monograph*, 29, 1984.

J. T. Kiehl and K. E. Trenberth. Earth's annual global mean energy budget. *Bulletin of the American Meteorological Society*, 1997.

R. Knutti and G. Hegerl. The equilibrium sensitivity of the earth's temperature to radiation changes. *Nature Geoscience*, 1, 2008.

A. Lahellec and J-L. Dufresne. A formal analysis of feedback concept in climate models: the inclusive feedback components. *not submitted*, 2011.

P. L. Langen and V. A. Alexeev. Polar amplification as a preferred response in an idealized aquaplanet gcm. *Climate Dynamics*, pages 305–317, February 2007.

J. Lu and M. Cai. Quantifying contributions to polar warming amplification in an idealized coupled general circulation model. *Climate Dynamics*, 34:669–687, 2010.

I. Medhaug and T. Furevik. North atlantic 20^{th} century multidecadal variability in coupled climate models: sea surface temperature and ocean overturning circulation. *Ocean Science Discussions*, 8:353–396, 2011.

D. M. Murphy, S. Solomon, R. W. Portmann, K. H. Rosenlof, and P. M. Forster. An observationally based energy balance for the earth since 1950. *Geophysical Research Letters*, 114, 2009.

R. T. Pierrehumbert. The hydrologic cycle in deep-time climate problems. *Nature*, 419, 2002.

S. Raper, J. M. Gregory, and R. J. Stouffer. The role of climate sensitivity and ocean heat uptake on an aogcm transient temperature response. *Journal of Climate*, 15: 124–130, 2002.

S.C.B. Raper, J.M. Gregory, and T.J. Osborn. Use of an upwelling-diffusion energy balance climate model to simulate and diagnose A/OGCM results. *Climate Dynamics*, 17:601–613, 2001.

S. E. Schwartz. Heat capacity, time constant, and sensitivity of earth's climate system. *Journal of Geophysical Research*, 112, 2007.

S. E. Schwartz. Feedback and sensitivity in an electrical circuit: an analog for climate models. *Climate Change*, 2010.

B. J. Soden and I. Held. An assessment of climate feedbacks in coupled ocean-atmosphere models. *Journal of climate*, 19, 2006.

B. J. Soden, A.J. Broccoli, and R. S. Hemler. On the use of cloud forcing to estimate cloud feedback. *Journal of climate*, 17, 2004.

J. S. Soden, I. M. Held, R. Colman, K. M. Shell, J. T. Kiehl, and C. A. Shields. Quantifying climate feedbacks using radiative kernels. *Journal of climate*, 21, 2008.

S. Solomon, D. Qin, M. Manning, Z. Chen, M. Marquis, K.B. Averyt, M. Tignor, and H.L. Miller. Climate change 2007: The scientific basis, supplementary material,chapter 8. *Cambridge university Press*, page 73, 2007.

R. J. Stouffer. Time scales of climate response. *Journal of climate*, 2004.

K. E. Trenberth, J. T. Fasullo, and Kiehl J. Earth's global energy budget. *American Meteorological Society*, 2009.

J. Turner, T. A. Lachlan-Cope, S. Colwell, G. J. Marshall, and W. M. Connolley. Significant warming of the antarctic winter troposphere. *Science*, 311, 2006.

D. G. Vaughan and C. S. M. Doake. Recent atmospheric warming and retreat of ice shelves on the antarctic peninsula. *Nature*, January 1996.

R. Wetherald, J. Stouffer, and Dixon K. Committed warming and its implications for climate change. *Geophysical Research Letters*, 28(8):1535–1538, 2001.

M. Winton. Amplified arctic climate change: What does surface albedo feedback have to do with it? *Geophysical Research Letters*, 33, February 2006.

M. Winton, K. Takahashi, and I. M. Held. Importance of ocean heat uptake efficiency to transient climate change. *Journal of Climate*, 231:2333–2344, May 2010.